

Copyright The University of Chicago 2019. Preprint (not copyedited or formatted).
Please use DOI when citing or quoting. DOI: 10.1086/704157

Coevolution Creates Complex Mosaics Across Large Landscapes

Lucas D. Fernandes^{1,*}

Paula Lemos-Costa²

Paulo R. Guimarães Jr.³

John N. Thompson⁴

Marcus A. M. de Aguiar⁵

1. Department of Life Sciences, Imperial College London, Silwood Park, Ascot, Berkshire, SL5 7PY, UK

2. Programa de pós-graduação em Ecologia - Instituto de Biologia, Universidade Estadual de Campinas, Unicamp, 13083-865, Campinas/SP, Brazil;

3. Departamento de Ecologia, Universidade de São Paulo, 05508-090, São Paulo/SP, Brazil;

4. Department of Ecology and Evolutionary Biology, University of California, Santa Cruz, CA 95064.

5. Instituto de Física “Gleb Wataghin”, Universidade Estadual de Campinas, Unicamp, 13083-859, Campinas/SP, Brazil;

* Corresponding author; e-mail: lucasd.fphys@gmail.com.

Manuscript elements: Figure 1, Figure 2 , Figure 3, Figure 4, Figure 5, Figure 6, online Supplementary Material (including figures A1–A6 and videos A1–A3). Figure 1, Figure 2, Figure 3, Figure 4, Figure 5, Figure 6 are to print in color.

Keywords: antagonisms, geographic mosaic of coevolution, mutualisms, phenotypic patterns,

selection patterns, species interactions.

Manuscript type: Article.

Prepared using the suggested L^AT_EX template for *Am. Nat.*

Abstract

The spatial distribution of populations can influence the evolutionary outcome of species interactions. The variation in direction and strength of selection across local communities creates geographic selection mosaics that, when combined with gene flow and genomic processes such as genome duplication or hybridization, can fuel ongoing coevolution. A fundamental problem to solve is how coevolution proceeds when many populations that vary in their ecological outcomes are connected across large landscapes. Here we use a lattice model to explore this problem. Our results show that the complex interrelationships among the elements of the geographic mosaic of coevolution can lead to the formation of clusters of populations with similar phenotypes that are larger than expected by local selection. Our results indicate that neither the spatial distribution of phenotypes nor the spatial differences in magnitude and direction of selection alone dictate coevolutionary dynamics: the geographic mosaic of coevolution affects formation of phenotypic clusters, which in turn affect the spatial and temporal dynamics of coevolution. Because the formation of large phenotypic clusters depends on gene flow, we predict current habitat fragmentation will change the outcomes of geographic mosaics, coupling spatial patterns in selection and phenotypes.

Introduction

One of the main questions at the interface of evolution and ecology is how species interactions shape the diversity of life (Thompson 2005). Evolution mediated by species interactions may influence speciation rates (Johnson 2010), extinction rates (van Valen 1973), spatial distributions (Alonso et al. 2002), community organization (Gotelli et al. 2010; Nuismer et al. 2013), and genetic (Wade 2007) and phenotypic (Guimarães et al. 2017) diversity. Deciphering how species interactions shape evolutionary rates and patterns, however, has been challenging, because each interaction between a pair of species is a collection of local interactions that may vary in ecological outcomes and fitness effects on the participants (Brodie et al. 2002; Gandon et al. 2008). The geographic mosaic theory of coevolution confronts this complexity by considering relationships between species as genotype by genotype by environment ($GxGxE$) interactions (Thompson 2005).

The sources of spatial variation can be partitioned in three main components that affect $GxGxE$ interactions and the resulting coevolutionary dynamics. First, the direction and magnitude of selection can vary across local communities, creating geographic selection mosaics (Brodie et al. 2002; Parchman and Benkman 2002). For example, *Greyia* moths are major pollinators of woodland star (*Lithophragma*) flowers that lay eggs in the same flowers they pollinate. The larvae eat very few seeds and the interaction is mutualistic in many environments. In some environments, however, the presence of co-pollinators that do not lay eggs in the flowers swamp the mutualism, making the interaction between the plants and *Greyia* moths antagonistic rather than mutualistic (Thompson and Cunningham 2002). Second, reciprocal selection may vary among environments, creating coevolutionary hotspots, where the interaction affects the fitness of both partners, and coevolutionary coldspots where selection is not reciprocal or there is no selection (Laine 2009). Finally, gene flow, hybridization, and genomic alterations can lead to trait remixing among populations as allele frequencies and the structure of genomes undergo continual reorganization in different ways in different populations (Lexer et al. 2013; Thompson and Merg 2008;

Whitham et al. 2006). Trait remixing results in variation among populations in the phenotypic distribution of traits available for natural selection (Dybdahl and Lively 1996). Collectively, selection mosaics, coevolutionary hotspots, and trait remixing can fuel ongoing coevolution in ways that differ from solely local coevolution in rates, trajectories, and patterns of phenotypic change (Nuismer et al. 1999).

The dynamics of coevolutionary mosaics have now been explored in mathematical models (Gibert et al. 2013; Lemos-Costa et al. 2017; Nuismer et al. 1999), laboratory microcosms (Forde et al. 2004; Vogwill et al. 2009), and natural communities (Gómez et al. 2009; Gómez and Buckling 2011; Parchman and Benkman 2002), but most studies have been limited to analysis of few populations relative to the full spatial complexity found in assemblages of coevolving species in nature. These studies, however, have shown that all three components of coevolutionary mosaics can contribute to discrepancies between the local patterns of natural selection and the local distribution of phenotypes. For example, at the local level, theory predicts that mutualisms would favor fixation of beneficial phenotypes, whereas antagonistic interactions may show unbounded oscillations of phenotype frequencies (Nuismer et al. 1999). In contrast, if an interaction is distributed across two ecologically contrasting sites linked by gene flow, mutualisms may not result in fixation of beneficial alleles at the local level and antagonisms may show damped oscillations of phenotypes or long-lasting clines along linear arrays of populations (Gomulkiewicz et al. 2000; Nuismer et al. 1999, 2000). Taken together, the available studies on coevolutionary dynamics indicate that spatial structuring results in qualitatively different outcomes than predicted by studies at single sites (Gibert et al. 2013; Lemos-Costa et al. 2017; Lion and Gandon 2015).

A current major problem to solve is how the consequences of the spatial organization of interactions scale up across large landscapes formed by hundreds or thousands of ecologically different sites rather than just a few sites (Thompson 2005). That is, how do the spatial scales of coevolutionary selection and gene flow shape the spatial scales of evolutionary outcomes? Here we integrate coevolutionary models, numerical simulations and tools derived from statistical mechanics to evaluate how coevolution proceeds between species whose interactions vary from

antagonism to mutualism across environmentally diverse landscapes. We show that coevolution across many ecologically diverse sites creates patterns in the distribution of coevolving traits that cannot be predicted by local selection alone or by models assuming simpler spatial organization. Specifically, we show that the interplay between selection mosaics, coevolutionary hotspots and coldspots, and trait remixing across large landscapes lead to the formation of regional groups of populations characterized by similar phenotypes that are larger than expected by the patterns of selection at local levels alone. The results show that complex patterns of trait matching and mismatching occur through the combined effects of selection mosaics and gene flow among coevolutionary hotspots. In addition, we show that these patterns may have statistical properties that are predictable, and thus may be explored with empirical data.

Methods

Model

We consider an $L \times L$ square lattice with periodic boundary conditions where each site represents a community with two species. Individuals of the two different species interact within sites and interactions can be mutualistic or antagonistic, depending on the site. Each site, however, is linked to its nearest neighbors and individuals of both species can migrate to connected sites. The sites are labeled (i, j) with $i, j = 1, 2, \dots, L$. Following (Nuismer et al. 1999), we model the species as haploid individuals and consider the interactions to be governed by a single locus with two alleles. As local populations are considered infinite, the dynamics acts upon the allelic frequencies, which is a reasonable simplifying assumption grounded in classical population genetics (Rice 2004). Species X, referred to as symbiont, has alleles A and a , with x_{ij} denoting frequency of allele A at site (i, j) , and species Y, referred to as host, has alleles B and b , with y_{ij} denoting frequency of allele B at site (i, j) . The symbiont always receives a fitness increase when interacting with matching alleles (A matches B and a matches b ; there are no cross interactions). Fitness increases or decreases for the host depend on the site. For the sites where the interac-

tion between the species is mutualistic (hereafter, mutualistic sites or mutualistic selection), the fitness of the host increases for matching alleles. Otherwise, for the sites where the interaction is antagonistic (hereafter, antagonistic sites or antagonistic selection), the fitness decreases for the host species when alleles are matched. For these analyses, we use the concepts of genotype and phenotype interchangeably, or in other words, we consider a direct relation between allele frequencies and corresponding traits (no environmental influence of the phenotypes). The selection mosaics are established at the beginning of the simulation and held fixed throughout the simulation. Each site is assigned as mutualistic with probability p and antagonistic with probability $(1 - p)$. Population fitnesses are modeled according to:

$$\begin{aligned} W_A^{(i,j)} &= 1 + Qy_{ij} \\ W_a^{(i,j)} &= 1 + Q(1 - y_{ij}) \\ W_B^{(i,j)} &= 1 + \gamma_{ij}x_{ij} \\ W_b^{(i,j)} &= 1 + \gamma_{ij}(1 - x_{ij}) \end{aligned} \tag{1}$$

where $W_\alpha^{(i,j)}$ is the fitness allele at site (i, j) and Q is the sensitivity of the fitness of the symbiont to changes in the allelic frequency of the host. Note that as the symbiont always receives a fitness increase from the interaction, $Q > 0$. The parameter γ_{ij} represents the sensitivity of the fitness of the host to changes in the allelic frequency of the symbiont and its value depends on the type of local interaction. We set $\gamma_{ij} = K_M > 0$ for sites with mutualistic interactions, in which interaction between matching alleles increases host's fitness, and $\gamma_{ij} = K_A < 0$, for sites with antagonistic interactions, in which interaction decreases host's fitness. We refer to K_M and K_A as the strengths of selection for mutualism and antagonism, respectively. Gene flow happens before selection with rate m , equally divided among the four nearest neighbors. With these assumptions, we have the following recurrence equations for the changes of frequencies x_{ij} and y_{ij} in each generation:

$$\begin{aligned} x_{ij}^{(n+1)} &= \frac{x_{ij}^{(n,*)} W_A^{(i,j)}}{x_{ij}^{(n,*)} W_A^{(i,j)} + (1 - x_{ij}^{(n,*)}) W_a^{(i,j)}} \\ y_{ij}^{(n+1)} &= \frac{y_{ij}^{(n,*)} W_B^{(i,j)}}{y_{ij}^{(n,*)} W_B^{(i,j)} + (1 - y_{ij}^{(n,*)}) W_b^{(i,j)}}, \end{aligned} \quad (2)$$

where

$$\begin{aligned} x_{ij}^{(n,*)} &= x_{ij}^{(n)}(1 - m) + \frac{m}{4} \sum_{(s,t)} x_{i+s,j+t}^{(n)} \\ y_{ij}^{(n,*)} &= y_{ij}^{(n)}(1 - m) + \frac{m}{4} \sum_{(s,t)} y_{i+s,j+t}^{(n)} \end{aligned} \quad (3)$$

are the allelic frequencies after gene flow (the summations over s and t are restricted to the four nearest neighbors). Note that the choice of local infinite population sizes provides a simplification that eliminates fluctuations from stochastic effects such as genetic drift, allowing the investigation of the effect of species interaction and coevolution in generating phenotypic patterns at the landscape scale in the absence of complicating factors. In all simulations, both x and y are initiated with values 0.51 for every site on the lattice, so that the differences in the phenotypic patterns arise due to spatial variation in the local interaction and to gene flow, not to variation in initial conditions among sites. The square lattice has size $L = 100$ and evolution occurs for 40,000 generations.

Mean-field with spatially varying carrying capacities

The balance between spatial prevalence of one interaction and local selection strength was further explored with a mean-field, two-sites approximation, in which each site has a carrying capacity representing the spatial prevalence over the landscape (parameters p for mutualistic sites and $(1 - p)$ for antagonistic sites in the landscape model).

The two-sites model proposed by Nuismer and coauthors (Nuismer et al. 1999) was modified to include different carrying capacities associated with each site (Lemos-Costa et al. 2017).

Specifically, we consider the situation in which the first site, where the interactions are mutualistic, has carrying capacity N_1 , whereas the second site, where the interactions are antagonistic, has carrying capacity N_2 . In this case the equations describing the gene flow between the sites change to:

$$\begin{aligned} x_1^{(n,*)} &= \frac{x_1^{(n,*)}(1-m)N_1 + x_2^{(n,*)}mN_2}{(1-m)N_1 + mN_2} \\ x_2^{(n,*)} &= \frac{x_2^{(n,*)}(1-m)N_2 + x_1^{(n,*)}mN_1}{(1-m)N_2 + mN_1}. \end{aligned} \quad (4)$$

These equations can be rewritten as:

$$\begin{aligned} x_1^{(n,*)} &= \frac{x_1^{(n,*)}(1-m)R + x_2^{(n,*)}m}{(1-m)R + m} \\ x_2^{(n,*)} &= \frac{x_2^{(n,*)}(1-m) + x_1^{(n,*)}mR}{(1-m) + mR} \end{aligned} \quad (5)$$

which depend only on the ratio $R = N_1/N_2$ between the carrying capacities of the mutualistic and antagonistic communities. We tested eight different values of R , going from $R = 1$ to $R = 0.3$ in intervals of 0.1. The equations for y_1 and y_2 are given by equivalent expressions. The selection equations are the same as the ones for the two-sites model (Nuismer et al. 1999).

To compare the results of the mean-field approach with the simulations on the lattice we define the variable C_j , which describes the behavior of the frequency of allele A (x_j) for each community j :

$$C_j = 2(x_j - 0.5) \quad (6)$$

When allele A is fixed, or close to fixation ($x \approx 1$), the community presents genotypic patterns in accordance with an isolated mutualistic community, and $C \approx 1$. When the allele A is close to 0.5 it presents the pattern expected from an isolated antagonistic community, and $C \approx 0$. Fixation of allele a ($x \approx 0$) would give $C \approx -1$. Finally, to compare the mean-field results with the spatial prevalence of mutualistic versus antagonistic communities in numerical simulations, we calculate the average value C_{AV} , which considers the size of each community:

$$C_{\text{av}} = \frac{N_1}{N_1 + N_2} C_1 + \frac{N_2}{N_1 + N_2} C_2. \quad (7)$$

The size of each community in the mean-field model is comparable to the number of sites with each local outcome of selection (mutualistic versus antagonistic) in the spatial model. Given that the parameter p is approximated by the frequency of mutualistic sites on the lattice, $p = N_M / (N_M + N_A)$, with N_M and N_A the numbers of mutualistic and antagonistic sites, respectively, and defining $R = N_M / N_A$, we have

$$R = \frac{p}{1 - p} \quad (8)$$

Thus, we can compare the ratio of the carrying capacities (R) and the probability of a given site to be mutualistic on the lattice (p), which are the determinants of the behavior transitions in their respective models, and check how well the mean-field describes the evolutionary outcomes on the spatial lattice.

Cluster and coldspots analyses

To count clusters of a given allele frequency we first define a frequency interval. For example, when counting clusters where the frequency of allele A is larger than 0.7, we start with a site where the allele frequency is in the selected interval. Next, the four nearest neighbors of that site are analyzed and, if their allelic frequency also belongs to that interval, they are added to the cluster. The neighbors of the neighbors are all analyzed, until no other sites are added, indicating the end of the process. This iteration is repeated until all sites on the lattice are visited. Isolated sites (for which none of the four neighbors belong to the same interval) are considered clusters of size 1. This process gives the numbers of clusters with all sizes in the chosen interval. Finally, we normalize the distributions by the total number of clusters found, for a given value of gene flow.

For the coldspots analysis, the selection mosaics are first built the same way as before, with

each site assigned as mutualistic with probability p and antagonistic with probability $(1 - p)$. A given fraction f of the sites is then chosen randomly and marked as coldspots, where the interaction favors the symbiont (with fitness effects being the same as in hotspots, i.e., $Q > 0$), but does not influence host's fitness (at coldspots, we have: $\gamma_{ij} = 0$ and $W_B = W_b = 1$). This process, however, changes the average fitness sensitivity of the host, $\bar{s}_{YC} = \frac{1}{L^2} \sum_{ij} \gamma_{ij}$, as the fraction of coldspots is increased (see Supplementary Material). To keep the average fitness sensitivity fixed as the fraction of coldspots is varied, the value of p for the initial selection mosaic has to be a function of f . Thus, for a fixed average fitness sensitivity of the host, \bar{s}_{YC} , for each value of f to be tested, the value of p is defined as:

$$p = \frac{1}{(K_M - K_A)} \left[\frac{\bar{s}_{YC}}{(1 - f)} - K_A \right] \quad (9)$$

Results

Spatial patterns for alleles A and B

Our analysis suggests that coevolutionary mosaics in large landscapes lead to unexpected large-scale phenotypic patterns that cannot be explained by local processes alone. The transient evolutionary trajectories produced pockets of high allele frequency and, after a few thousand generations, the spatial patterns stabilized and became stationary. We begin our analysis on the stationary patterns of allele A and B frequencies (symbiont and host species, respectively) across the landscape.

We first explored how gene flow affects the distribution of allele A frequencies when mutualism increasingly dominates the landscape. In these scenarios, we varied the proportion of mutualistic sites, keeping the intensity of selection fixed and twice as high for the host species in mutualistic sites than in antagonistic sites ($|K_M| = 2|K_A|$). Under these conditions, different combinations of selection mosaics and gene flow resulted in substantially different large-scale spatial patterns of allele A distributions (Fig. 1). Although we have iterated the process for

40000 generations, to guarantee stationarity for all parameter sets, the majority of sites on the landscape settled on the final allele frequencies much earlier (in many cases, before 3000 generations; see Supplementary Material). At low rates of gene flow ($m = 0.002$, Figs. 1(b), (f), and (j)) the spatial distribution of frequency of alleles mirrored the distribution expected by the local pattern of selection: antagonistic sites maintained polymorphic populations, whereas mutualistic sites showed allele fixation. When the proportion of antagonistic sites was higher than that of mutualistic sites ($p = 0.25$), the spatial prevalence of antagonistic sites compensated for the stronger intensity of selection at mutualistic sites. As a result, polymorphism remained prevalent throughout the landscape (Fig. 1(d)).

Figure 1: figure approximately here

Large and stable regional groups of high allele frequencies developed as the proportion of mutualistic sites and gene flow increased. These stable clusters of high allele frequencies locally shielded those sites from the oscillatory dynamics generated by local antagonistic selection (Fig. 1(d)). As the proportion of mutualistic sites and the rate of gene flow increased, the landscape began to appear as if mutualism were ubiquitous, even though the interaction was antagonistic at some sites (Figs. 1(h) and (l)). The effects of cluster shielding and consequent loss of resolution of fine structures on the mosaic can be further investigated if we consider ordered structures for the spatial distribution of antagonistic and mutualistic sites. Block and gradient mosaics are useful to understand how gene flow affects allele clines on the boundary of different selection regions, as well as how gene flow and selection mosaic clusters influence the loss of resolution of spatial structures on the final phenotypic patterns (see Supplementary Material).

The stationary distributions for allele B frequencies reveal similar patterns, obtained with the same underlying spatial structure of selection mosaics and the same parameters as before, but with important differences. At low rates of gene flow ($m = 0.002$, Figs. 2(b), (f), and (j)) the spatial distribution of allele frequencies leads to allele fixation at mutualistic sites and polymorphism at antagonistic sites. The most striking differences in comparison with the patterns for allele A

appear as gene flow increases. When antagonistic sites are common ($p = 0.25$), a high level of gene flow ($m = 0.050$; Fig. 2(d)) also maintains a polymorphic state throughout the landscape. In contrast to the patterns observed for allele A , the characteristic sizes of the clusters where the frequency of allele B is close to fixation (orange and red spots) is notably reduced (compare with Fig. 1(d)). The clusters of low frequencies of allele B are also smaller. Clusters of fixation or low frequencies of allele B are located at the same approximate positions as the corresponding clusters of fixation or low frequencies of allele A .

Figure 2: figure approximately here

Increasing values of prevalence of mutualistic sites ($p = 0.50$) leads to a significant increase in the characteristic sizes of clusters of fixation of allele B (red spots). However, even with the largest value considered for gene flow ($m = 0.050$; Fig. 2(h)) polymorphic clusters are still present on a large portion of the landscape when mutualistic and antagonistic sites are equally prevalent. Several small clusters of low frequencies of allele B (blue spots) are also present in this scenario, These clusters were not observed for allele A under the same values for the proportion of mutualistic sites, p , and gene flow, m (Fig. 1(h)). Overall, when mutualistic sites are highly prevalent ($p = 0.75$), complete landscape-wide fixation of allele B is not accomplished even for the highest value of gene flow (Fig. 2(l)).

When scaled up into large landscapes, our modeling approach shows effects and patterns that substantially deviate from the theoretical predictions derived from two-site models in two fundamental ways. First, even for high rates of gene flow, local antagonistic clusters shield the effects of mutualisms, thereby leading to local aggregations of populations where alleles A and B are not fixed (yellow spots in Figs. 1(g), (h), and (k); also, Fig. 2(l)). Second, unlike in two-site models, sites with low frequencies of alleles A and B can occur (blue spots in Figs. 1(c) and (d); also, Figs. 2(h) and (k)) even though the initial frequencies of these alleles are higher than of alleles a and b for all the sites. In these large landscapes, the average size of these blue spots changes for different rates of gene flow (see video on the Supplementary Material).

Patterns of host's local adaptation in coevolutionary and single-species models

To separate the roles played by the underlying spatial mosaic structure (mutualistic and antagonistic sites' spatial distributions) and by the coevolutionary dynamics on the final phenotypic patterns, we next fixed $x_{ij} = 1$ throughout the landscape (allele A fixed in all sites). This is analogous to a local adaptation model for one species (Lenormand 2002), in which allele B has a fitness $1 + |K_M|$ at the sites assigned for mutualism and fitness $1 - |K_A|$ at sites assigned for antagonism (allele b has fitness 1 in all sites). We used the same selection mosaics used in Figs. 1 and 2 and compared the patterns obtained for the single-species model (Fig. 3) with the ones obtained for the two-species coevolutionary model (Fig. 2). As the proportion of mutualistic sites on the landscape reaches high values ($p = 0.50$ and $p = 0.75$), increasing gene flow makes the patterns for allele B on the single-species model nearly identical to the patterns for the coevolutionary model. This occurs because, at this high proportion of mutualistic sites, and with $|K_M| = 2|K_A|$, high rates of gene flow lead to a nearly complete fixation of allele A on the landscape (Figs. 1(h) and (l)).

Figure 3: figure approximately here

For a low level of mutualistic prevalence on the landscape ($p = 0.25$), the distinction between the patterns is more clearly noted. For the coevolutionary model the antagonistic sites tend to a state of polymorphism between alleles B and b (Figs. 2(a), (b) and (c)), whereas for the single-species model the sites where allele b has a fitness advantage over allele B (which are exactly the antagonistic sites on the previous model) reach a state of fixation or near-fixation of allele b (white sites - Figs. 3(a), (b) and (c)). For high levels of gene flow, the position and shape of the clusters of high allele B frequency (yellow and orange sites) are similar in both cases (Figs. 2(d) and 3(d)), indicating that the spatial structure of the selection mosaic influences the spatial arrangement of the final pattern. Nevertheless, the dynamics underlying the coevolutionary version of the model play a fundamental role in determining the regions of polymorphism or allele fixation.

The coevolutionary model results in less spatial structure than the single-species model with respect to the landscape-wide polymorphic pattern (Fig. 2(d)), as many of the mutualistic sites tend to the polymorphic state for high gene flow. It is still possible to distinguish more easily the sites for which selection is beneficial or detrimental for allele B on the single-species model, since the sites in which selection is beneficial for B resist fixation of b (compare blue sites in Fig. 3(d) with structure of the mosaic, Fig. 3(a)).

Gene flow, spatial structure and coldspots

We next explored how information is transferred from selection acting in one species (mutualistic or antagonistic selection on the host) to phenotypic evolution on the other (symbiont) species as a result of the interaction by focusing our attention on the patterns obtained for allele A . We analysed the effects of gene flow, spatial selection structure and the presence of evolutionary coldspots on these final patterns.

As the proportion of mutualistic sites increases, the relationship between gene flow and the fraction of sites near fixation of allele A changes from hump-shaped to a monotonic increase (Fig. 4(a)). For $p = 0.25$ and starting with small values of m , increasing gene flow results in an initial tendency of increasing the number of sites showing fixation of allele A . However, this locally strong influence of mutualism is compensated by the spatial prevalence of antagonistic sites, leading the majority of sites to retain polymorphism for higher values of gene flow. This hump-shaped relationship is also seen for $p = 0.30$, although the decay towards polymorphism for increasing values of gene flow is slower. For higher values of p , increasing values of gene flow always leads to increasing values of the fraction of sites with allelic frequencies of A near-to-fixation. For $p = 0.50$ or higher, even for intermediate values of gene flow a significant fraction of the lattice presents high values of the frequency of A (compare with Figs. 1(g) and (k)).

Figure 4: figure approximately here

The combined effects of the proportion of mutualistic sites, the relative strengths of mutual-

istic and antagonistic selection, and gene flow create two possible behaviours for the tendency to fixation of allele A (Fig. 4(a)). One is a monotonic increase in the fraction of near-to-fixation sites, as gene flow increases, until all lattice presents the same phenotypic patterns (for $p > 0.35$). The other is an initial increase of the fraction of near-to-fixation sites with subsequent decrease, leading to the polymorphic state, for high rates of gene flow (for $p < 0.30$). These outcomes suggest the existence of a threshold value for p , which would mark the transition between these different scenarios. Indeed, we derived the expression that shows that the transition between the tendency to polymorphism versus the tendency to allelic fixation, as gene flow increases, is governed by the value of the average sensitivity experienced by the host species, \bar{s}_Y (see Eq. S3, on the Supplementary Material). When \bar{s}_Y is negative, the landscape tends to polymorphism for large values of gene flow, whereas it tends to fixation when s_Y is positive. For the values of interaction strengths used ($K_M = 0.04$ and $K_A = -0.02$), the transition between these two tendencies occurs at $p = 0.33$, when $\bar{s}_Y = 0$ (see Eq. S3).

The tendency towards fixation or polymorphism is also observed in the mean-field model (Fig. 4(b)). When both communities have the same size ($R = 1$), the larger selective strength of mutualism compared to antagonism is enough to spread the tendency towards fixation (i.e., C_{AV} approaches 1), which characterizes the mutualistic community. If the size of the mutualistic community is slightly reduced, for $0.80 < R < 0.90$, the pattern still tends towards fixation as gene flow increases. In these cases, the strength of the mutualistic interaction has a stronger effect when compared to community size. Further reductions in the size of the mutualistic community lead to a drastic change in the behaviour of the system, with both communities tending towards polymorphism ($C_{AV} = 0$) as the gene flow increases when $R < 0.60$.

The results of the mean-field approach are therefore qualitatively similar to those obtained for the spatial case, with a clear transition between two states of allelic diversity. In addition, the two frameworks (spatial and mean-field) also suggest that even under strong mutualistic selection and high gene flow, polymorphisms can persist. In the spatial model, persistence occurs if antagonistic sites are predominant across the landscape when considering all sites or, in the

case of the mean-field, if the size of the antagonistic community is greater than the size of the mutualistic community. However, the value of R that seems to mark the transition between the two behaviours on the mean-field model ($R \approx 0.7$) is not exactly the same that would be expected through direct comparison with the value of p for the transition on the lattice model (in Eq. 8, for $p = 1/3$ one would expect $R = 0.5$). Even though an exact quantitative comparison with the spatial case is not possible in this approximation, the mean-field model succeeds in depicting a transition between two possible coevolutionary outcomes, similar to that found on the spatial case.

Figure 5: figure approximately here

A closer analysis of the size of mutualistic clusters suggests a relationship between the structure of the geographic selection mosaic (i.e., the distribution and the relative proportion of mutualistic and antagonistic sites) and the size of phenotypic clusters. In the absence of gene flow, the frequencies of clusters with high allele frequency coincide with the frequencies of mutualistic clusters for both A and B (Figs. 5(a) and (b)). Increasing gene flow increases not only the mean cluster size, but also the probability of finding a cluster of allele fixation larger than expected from the spatial distribution of mutualistic sites (Fig. 5). However, a clear distinction can be noted on the changes in cluster frequencies for alleles A and B as gene flow increases. As shown before for the spatial patterns (Figs. 1 and 2), the characteristic sizes of the clusters where the frequency of allele B is close to fixation (greater than 0.7) is smaller than sizes of clusters on the same interval for allele A for the same gene flow rate. The interval of sizes of clusters close to fixation is also significantly broader for allele A (Fig. 5(a)), for all values of gene flow. Important differences in cluster frequencies can also be shown when comparing allele B frequencies on the coevolutionary and single-species models (see Figs. S5 and S6 in Supplementary Material).

From the results of cluster frequencies (Fig. 5) we note that fixation of alleles throughout a landscape depends on the combined effects of the spatial distribution of mutualistic and antagonistic sites, forming the selection mosaics, and the rate of gene flow, also presenting important

differences between interacting species. These results lead to two main predictions: first, the presence of phenotypic clusters with variable sizes across landscapes might hide the outcomes of the interactions at finer spatial scales (phenotypic clusters of allele fixation might be formed by many sites where the interaction is antagonistic, for example). Second, the presence of phenotypic clusters with broad variation in sizes might actually be a signature that a non-regular spatial structure of small and medium size clusters of mutualistic and antagonistic sites are shaping phenotypic evolution in a coevolutionary context (regular structures with equal sizes, even if there were many, would not allow the formation of broad distributions of phenotypes; compare these phenotypic patterns with the ones obtained from regular block mosaics on the Supplementary Material).

Figure 6: figure approximately here

Finally, we added to these large landscapes the third component of geographic mosaics: coevolutionary hotspots and coldspots. In the coevolutionary coldspots, the interaction affected the evolutionary dynamics of the symbiont but not the host (i.e., $\gamma_{ij} = 0$ representing the absence of interaction effect on fitness of species Y). In other words, coldspots represent communities where the symbiont was commensalistic on its host. We distributed coevolutionary coldspots among the antagonistic and mutualistic sites. We then explored the effects of the proportion of coldspots and the rates of gene flow on the frequency of sites with high frequencies of alleles A ($x > 0.7$), as we kept the average fitness sensitivity of the host fixed. For fixed values of gene flow, the tendency towards allelic fixation on the symbiont depended on the average value of the fitness sensitivity of the host. For a negative average fitness sensitivity (Fig. 6(a)), increasing the fraction of coldspots led to a decrease in the number of sites with high frequencies of allele A . In contrast, for a positive average fitness sensitivity (Fig. 6(c)) the increase in the fraction of coldspots led to an increase in the number of sites with high allele A frequencies.

The effect of coldspots follow from the influence of the mutualistic clusters on the initial selection mosaics. Because the probability p for the initial selection mosaic is a function of f ,

so that the average fitness sensitivity is fixed (see Methods and Supplementary Material), the variation of p is dependent on the value of the average fitness. For $\overline{s_{YC}} < 0$ (Fig. 6(a)), p is a decreasing function of f : with $\overline{s_{YC}} = -0.005$, as f increases from 0.0 to 0.5, p decreases from 0.25 to 0.17. In contrast, for $\overline{s_{YC}} > 0$ (Fig. 6(c)), p is an increasing function of f : with $\overline{s_{YC}} = 0.005$, as f increases from 0.0 to 0.5, p increases from 0.42 to 0.50. For $\overline{s_{YC}} = 0.0$, p is independent of f , and thus the number of sites presenting high allele A frequencies should depend only on the value of the gene flow. However, it is possible to note a slight increase in the number of sites with high allele A frequencies as f increases (Fig. 6(b)). This is mainly due to the fact that the lattice is finite and the selection of coldspots is slightly biased towards antagonistic sites in this case. Hence, the proportion of coldspots in a landscape alters the outcome of the interaction in different ways that depend on the landscape proportions of mutualistic and antagonistic sites as well as on fitness sensitivity of the interacting species.

Discussion

Previous studies have been successful in describing the evolutionary forces that drive the formation of single-species clines in traits (Felsenstein 1976; Lenormand 2002; Nagylaki 1975; Slatkin 1978). Adding to the vast literature of local adaptation in single species, subsequent studies have also investigated the formation of evolutionary clines in one-dimensional systems of coevolving species (Nuismer et al. 2000). Here we have shown that novel dynamics result when species co-evolve across large landscapes over which the interactions vary from antagonism to mutualism, forming a geographic selection mosaic of ecological outcomes. These novel dynamics produce geographic clusters of similar phenotypes, resulting from a combination of the geographic mosaics, the distribution of coevolutionary hotspots and coldspots, and the degree and pattern of gene flow.

Direct comparison between the 2-species and single-species models indicated that, for small fractions of mutualistic sites in the landscape ($p = 0.25$), significant differences appeared for

allele composition on antagonistic sites. Whereas polymorphic states are observed with notable spatial predominance in the coevolutionary case, for the single-species model polymorphism is associated with the transition between regions of near fixation of allele *B* and near fixation of allele *b*. As a consequence, major differences also appear in the cluster distributions for allele *B* in these two models (Figs. S5 and S6).

These results imply that the two main drivers for the formation of the patterns we describe are the two-dimensional topology of the selection mosaics, which influences position and sizes distribution of the phenotypic clusters, and coevolutionary dynamics, which directly affect the maintenance of fixation and polymorphism on the landscape. Our results therefore expand current local adaptation theory by showing that (i) a large bidimensional landscape serves as a stage for the formation of a broad size distribution of mutualistic and antagonistic clusters, which are directly linked to the formation of phenotypic clusters that vary non-linearly in size with gene flow (see Fig. 5), and (ii) maintenance of polymorphisms in large ecologically complex landscapes is significantly altered by coevolutionary dynamics, and depends on the rate of gene flow and the spatial prevalence of mutualism or antagonism.

In this work we isolated how the spatial scales of selection and gene flow affect the spatial scale of adaptation and coadaptation when interactions vary from antagonism to mutualism within a large landscape. This analysis was performed by focusing mostly on allele *A*, but our analyses also showed that the dynamics of allele *B* differ in some respects from those found in *A*. A deeper analysis of the patterns of allele *B* would also be important, as well as investigating how the mismatch between interacting alleles *A* and *B* is dependent on gene flow and spatial structure. However, these analyses introduce another set of effects that need to be evaluated in a truly robust way, which goes beyond the scope of this paper.

Our results are directly relevant to understanding the structure of coevolving interactions found in nature. Selection mosaics, coevolutionary hotspots, and variable frequencies of coevolving traits have been observed in nature at a wide range of spatial scales (Thompson 2013). Moreover, geographic mosaics in coevolutionary selection have been previously shown to be

an important ingredient in the formation of evolutionary patterns. For example, observed geographic mosaics range from mosaics of ecological outcomes or traits (e.g., Benkman et al. 2001; Brodie et al. 2002; Thompson and Cunningham 2002) to clinal patterns in traits, such as in the interaction between camellias (*Camellia japonica*) and camellia weevils (*Curculio camelliae*) along latitudinal and elevational gradients in Japan (Toju et al. 2011). Our work opens the opportunity to investigate the underlying processes shaping coevolving interactions in the large and more complex landscapes found in other interactions.

In one-dimensional models of geographic mosaics, the most likely outcome is the evolution of clines (Nuismer et al. 2000). Our results for the analyses of large landscapes suggest three extensions of coevolutionary theory. First, the interplay between spatial structure, gene flow and selection mosaics can lead to the formation of clusters of allelic frequencies that differ significantly from those expected by the spatial distribution of mutualistic and antagonistic sites. On the local level, one would expect fixation of alleles on mutualistic sites and polymorphism on antagonistic sites. Our results show instead a marked discrepancy between the final allelic frequencies and that expected by local selection regimes at finer spatial scales. These results support the view that all three components of the geographic mosaic of coevolution - selection mosaics, hotspots, and trait remixing - should be considered when investigating how species interactions shape evolution of alleles and traits (Thompson 2005). Empirical work has described the spatial structure of magnitude and direction of selection, as well as the distribution of phenotypes of several coevolved species interactions (Brodie et al. 2002; Parchman and Benkman 2002; Ruano et al. 2011). Some of these studies have revealed clusters of populations sharing similar trait patterns, in which a mismatch between phenotypic patterns and selection often occurs (Hanifin et al. 2008; Nogueira et al. 2015). Previous work associates this pattern with differences in responses of interacting species to coevolutionary selection (Hanifin et al. 2008) or to similar directional selection across space (Benkman and Parchman 2013). Our study provides an additional mechanism that may contribute to these spatial patterns: the formation of trait clusters as a consequence of gene flow amplifying local selection and generating a distribution of clusters of phenotypes.

Second, a key aspect of the disparity between the spatial distribution of the selection mosaics and the resulting phenotypes is the formation of local clustering of sites showing similar allele frequencies. We provide a mechanism for this departure in allele distributions by hypothesizing that aggregations of sites with similar selective regimes shield the effects of stronger interaction strength and/or higher prevalence of other selective regimes, leading to the formation of the phenotypic clusters. Nuismer and coauthors (Nuismer et al. 2000) reported a shielding effect in their linear spatial model of coevolution. By generalizing coevolutionary models to two-dimensional lattices our study shows that this shielding effect leads to the formation of clusters of multiple sizes across the landscape. Together these results suggest that shielding effects may be a common feature of coevolution for interactions with a geographic mosaic structure. The comparison with the mean-field results also suggests the relevance of numerical effects and spatial structure to understanding these final distributions of phenotypes. These analyses suggest that coevolution across space favors the formation of discrete regional groups of populations sharing similar phenotypes, even if selection mosaics are not spatially organized. In this sense, the statistical properties of the distribution of cluster sizes provide information on the role of gene flow in reshaping the patterns of traits predicted by selection mosaics. Additionally, our model predicts a wide variation in cluster sizes within metapopulations of interacting species, in agreement with empirical evidence supporting the notion that cluster patterns in traits and allele frequencies can occur on scales varying from a few square kilometers or less (King et al. 2009; Koskella et al. 2011; Laine 2009) to scales of tens or hundreds of square meters or more (Anderson and Johnson 2008; Benkman et al. 2010; Burdon and Thrall 2014; Hanifin et al. 2008; Pennings et al. 2009).

Third, we show that coevolutionary coldspots may change evolutionary dynamics by modulating the effects of gene flow, favoring particular allele frequencies and changing the consequences of the selection mosaics. Recent work shows that the spatial organization of coldspots and hotspots affects the polymorphism persistence in small spatial networks of two antagonistic species (Gibert et al. 2013). By incorporating the fact that mutualisms and antagonisms are often the endpoints of a continuum of variable fitness consequences (Thompson 2005), the asymmetry

in selection that characterizes coldspots favors an asymmetry of the distribution of alleles at the landscape level, thereby maintaining allele diversity (and polymorphism) in the host populations over large spatial areas.

More generally, the results suggest how future theoretical and empirical studies could explore the statistical properties of cluster of traits and selection mosaics within metapopulations of interacting species. Selection mosaics incorporated into metacommunity structure show that central communities might play a disproportionate role in coevolutionary dynamics (Lemos-Costa et al. 2017). When scaled up to the landscape level, we hypothesize that the spatial effects described here will amplify the formation of clusters of high or low allele frequencies in nature. The formation of discrete regional groups is a form of a broad class of spatial processes which occur in biological and physical systems (Alonso et al. 2002; Liu et al. 2010). In this sense, this work represents a step in creating a bridge between coevolutionary theory (Thompson 2005) and the study of spatial processes in dynamical systems (Murray 2011).

We have incorporated two important simplifying assumptions in our model, namely infinite population sizes and haploid organisms. Infinite population sizes enable us to work exclusively with gene frequencies, focusing our analysis on the dynamical effects of frequency dependent selection and controlling for the stochasticity inherent of finite population sizes. It is important to note that this assumption holds as long as the number of migrants is small compared to the local populations on a finite case. If the numbers of migrants is large, dynamical instabilities associated with the formation of the final patterns would likely lead to different dynamical regimes from the stationary patterns discussed here. A robust analysis of these regimes, considering demographic dynamics of varying population sizes in space and, consequently, asymmetric rates of gene flow, would be an important extension of our work that would permit an understanding of how eco-evolutionary dynamics affect the spatial distribution of phenotypes. Additionally, diploid traits might introduce an additional source of local diversification even under the influence of strong mutualistic selection, which has been shown to prevent diversification in many cases (Raimundo et al. 2014).

Finally, these results provide a framework for future studies to explore the coevolutionary consequences of human-driven habitat fragmentation and loss in natural landscapes. Although we focus mainly on the final stationary patterns of allelic distributions, the transient evolutionary dynamics are important and relevant, especially nowadays as environments worldwide are undergoing rapid change. The results of this study also reinforce the difficulty of interpreting the spatial structure of interaction outcomes and future trajectories in coevolving interactions based on analyses focusing only on local and small-scale allele frequencies, even after hundreds of generations. For now, we predict that habitat fragmentation, by reducing rates of gene flow across landscapes, is likely to impede the formation of larger clusters of populations with similar phenotypes, thereby making the spatial structure of phenotypes (distribution of phenotypic clusters) more similar to the structure of selection mosaics (clusters of mutualism or antagonism).

Acknowledgments

The authors would like to acknowledge the funding provided by the European Union Seventh Framework Programme [FP7/2007-2013] (NICHE; grant agreement 289384) (L.D.F.), the São Paulo Research Foundation (Fundação de Amparo à Pesquisa do Estado de São Paulo) (P.R.G. - grant 2009/54422-8 -, M.A.M.A. - grant 2016/06054-3 - and L.D.F. - grant 2015/26989-4), the National Council of Scientific and Technological Development (CNPq) (M.A.M.A. and P.L.C.) and the National Science Foundation (NSF) (J.N.T - DEB-0839853).

Appendix: Online Supplementary material

Fitness sensitivity across the landscape – mean and variance

Regular model without coldspots

We calculate the mean and variance of the fitness sensitivities across the landscape for both interacting species. If \bar{s}_X and σ_X^2 are the mean and variance for the symbiont sensitivities, respectively, we have:

$$\bar{s}_X = Q \quad (\text{A1})$$

$$\sigma_X^2 = 0, \quad (\text{A2})$$

since there is no variation on symbiont sensitivities across the landscape.

The scenario is different for the host, for which the sensitivity is equal to K_M in mutualistic sites and K_A in antagonistic sites. If \bar{s}_Y and σ_Y^2 are the mean and variance for the host sensitivities, respectively, we have:

$$\begin{aligned} \bar{s}_Y &= K_M p + K_A (1 - p) \\ &= K_A + p(K_M - K_A) \end{aligned} \quad (\text{A3})$$

$$\begin{aligned} \sigma_Y^2 &= \bar{s}_Y^2 - (\bar{s}_Y)^2 \\ &= [K_M^2 p + K_A^2 (1 - p)] - [K_A + p(K_M - K_A)]^2 \\ &= (K_M - K_A)^2 p(1 - p) \end{aligned} \quad (\text{A4})$$

Model with coldspots

For the coldspots analysis, the selection mosaics are first built the same way as before, with each site assigned as mutualistic with probability p and antagonistic with probability $(1 - p)$. A fraction f of the sites is then chosen randomly and marked as coldspots, where the interaction favors the symbiont (with sensitivity equal to Q) and is indifferent to the host (with sensitivity equal to 0). Thus, the mean and variance for the symbiont sensitivities remain equal to Q and 0, respectively. For the host sensitivities, we have:

$$\begin{aligned}\overline{s_{Y^C}} &= K_M p(1 - f) + K_A(1 - p)(1 - f) \\ &= [K_A + p(K_M - K_A)](1 - f) \\ &= \overline{s_Y}(1 - f)\end{aligned}\tag{A5}$$

$$\begin{aligned}\sigma_{Y^C}^2 &= \overline{s_{Y^C}^2} - (\overline{s_{Y^C}})^2 \\ &= [K_M^2 p(1 - f) + K_A^2(1 - p)(1 - f)] - (1 - f)^2[K_A + p(K_M - K_A)]^2 \\ &= (1 - f)[(K_M - K_A)^2 p(1 - p) + f(K_A + p(K_M - K_A))^2] \\ &= (1 - f)[\sigma_Y^2 + f(\overline{s_Y})^2]\end{aligned}\tag{A6}$$

Note that the mean and variance of host sensitivities in the coldspots model (respectively, $\overline{s_{Y^C}}$ and $\sigma_{Y^C}^2$) are related to the mean and variance of host sensitivities in the model without coldspots (respectively, $\overline{s_Y}$ and σ_Y^2).

Alternative selection mosaics

In an attempt to understand particular features of the randomly constructed selection mosaics, we investigated two different scenarios: block mosaics and gradient mosaics.

Block mosaics

Block mosaics are the simplest approach to capture the influence of local clusters, and the shielding effect that the local prevalence of a given interaction type has over the dynamics of allele frequencies. We build the selection mosaic again as a 100×100 regular square lattice, in which the lower part of the lattice is formed only by antagonistic sites, while the upper part is formed by mutualistic sites (Fig. A1(a)). Sites are indexed by the index k , starting from the leftmost site on the first row of the lower part of the lattice. Thus, the first row has indexes going from 1 to 100, second row, 101 to 200, and so on until the upper part of the lattice is reached. Periodic boundaries conditions are used and the dynamics of the model are the same as explained in the main text.

Figure A1: figure approximately here

The first result to notice is the reinforcement produced by the clusters to the dynamical tendencies of single isolated sites. Isolated mutualistic sites tend to the fixation of the predominant alleles, while antagonistic sites tend to produce oscillations with increasing amplitudes. However, as mutualistic selection has, in this case, twice the strength of the antagonistic selection, we expected that for a given rate of gene flow, the increasing amplitude in the antagonistic communities would be reverted to damped oscillations and, possibly, fixation of the initially predominant alleles. This transition from increasing to decreasing amplitudes in the allelic oscillations in the antagonistic communities in fact appears, for this particular set of parameters and lattice size, for a value of gene flow $m \approx 0.056$.

Analysis for the final (average) frequencies of allele A on the lattice (Fig. A1(b)) shows that clines starting in the middle of the antagonistic cluster until the middle of the mutualistic cluster become less steep as gene flow increases (horizontal steps on the curves all have a length equal to 100 and indicate that nodes on the same line of the lattice present the same final frequencies). The decrease in steepness on the border of the clusters is directly related to the increase in correlation length induced by the increase in gene flow.

Figure A2: figure approximately here

Comparison between the sizes of the strictly fixed domain ($x_k = 1$), in the mutualistic cluster, and the fully polymorphic domain ($x_k = 0.5$), in the antagonistic cluster, reveals that the latter is reduced, compared to the former, as gene flow increases. This spread in the tendency to fixation, however, finds resistance in the antagonistic cluster, even for large rates of gene flow, as we described before as shielding effect. Fig. A2 shows the spatial patterns relative to the clines in Fig. A1(b) for comparison.

Gradient mosaics

A more complex spatial structure can be obtained defining the selection mosaic as a gradient, that goes from antagonistic predominance to mutualistic predominance on the landscape. Fig. A3 shows one possible gradient mosaic. The coevolutionary dynamics are again set as before, with the same parameters as in Fig. A1. Boundary conditions are also periodic. The final stationary outcomes for the spatial distribution of allele A are shown in Fig. A4 for different values of gene flow.

Figure A3: figure approximately here

Starting from small values of gene flow, it is possible to see how the spatial pattern goes from an intricate mixture between local allelic fixation and polymorphism (Fig. A4(a)), to a smooth pattern with well defined regions (Fig. A4(d)), as gene flow increases. The pattern for Fig. A4(a) still keeps the same spatial characteristics found in the completely random selection mosaic for the same gene flow rate (see Fig. 1, in the main text), with local groups of fixation associated to the clusters of mutualistic sites in the selection mosaic, and the appearance of sites with low frequencies of allele A (dark blue spots), associated with 1-site clusters of mutualistic sites isolated in antagonistic bigger clusters. The pattern for the largest value of gene flow (Fig. A4(d)) shows a well marked separation between the region for allelic fixation (upper part of the mosaic)

and the region of polymorphism (lower part of the mosaic), despite the presence of antagonistic sites in the upper region and mutualistic sites in the lower region. The increase in gene flow marks the increase in correlation lengths, reducing the effective importance of the fine structure of the mosaic in influencing the final patterns of allelic distribution. This lack of resolution for fine structures makes the outcomes of the gradient mosaics closer to the outcomes of the block mosaics (Fig. A2(d)) for sufficiently high values of gene flow.

Figure A4: figure approximately here

Cluster frequencies for allele B: coevolutionary and single-species models

Differences on the spatial patterns for allele *B* in the coevolutionary and single-species models (Figs. 2 and 3 of the main text, respectively) can be quantitatively assessed by the cluster frequencies in two different allelic frequency intervals. Figure S5 shows the comparison for the cluster frequencies in these two models for clusters in which $y > 0.7$. Figure S6 shows the same analysis for the interval $0.3 < y < 0.7$.

Figure A5: figure approximately here

Figure A6: figure approximately here

A comparison between the frequencies of clusters close to fixation ($y > 0.7$) in the coevolutionary and single-species models shows that while in the coevolutionary model (Fig. A5(a)) increasing the gene flow rate leads to an increase in the likelihood of clusters close to fixation larger than expected by the histogram of mutualistic clusters (diamonds in Fig. A5), the same increase in gene flow leads to a decrease in the frequency of clusters close to fixation for almost all sizes in the single-species model (Fig. A5(b)).

As discussed in the main text, increases in gene flow produce an increasing dominance of the polymorphic state ($0.3 < y < 0.7$ - see inset in Fig. A6(a) for increase in size and likelihood of the

larger cluster of polymorphism) in the lattice for the coevolutionary model. On the other hand, the same increase in gene flow in the single-species model (Fig. A6(b)) produces a spatial pattern marked by regions of fixation of allele B (associated to the largest clusters in which selection favours this allele) and regions of fixation of allele b (where selection favours allele b instead). Polymorphism in the single-species model is then associated with the transition regions between regions of allelic fixation, with increasing likelihood of larger polymorphic clusters as gene flow increases (Fig. A6(b)). The spatial distribution of polymorphism thus constitutes one of the most striking differences between the spatial outcomes for the frequencies of allele B in these two models.

Supplementary videos

Gene flow effect

In the video *pattern_A_gene_flow* we show two panels: the selection mosaic relative to $p = 0.25$ (mutualistic sites are shown in black and antagonistic sites, in light gray), on the right side, and the stationary phenotypic patterns, after the total simulation time, for allele A (frequency x), on the left, for different values of the gene flow rate, m . The other parameters are $K_M = 0.04$, $K_A = -0.02$ and $Q = 0.02$ and are left constant.

Note how the final pattern of x changes with the increase of the gene flow rate. This video corresponds to the same results shown in Fig. 4(a), for $p = 0.25$. Also worth noting is how the sizes of the blue domains (predominance of allele a) increase with m . For different values of m , blue spots appear on the lattice associated with different sizes and displacements of groups of mutualistic sites. This effect is not trivial and it only appears when considering this spatial feature on large landscapes.

Transient dynamics

The videos *transient_x_km004_ka002_m0015_p025* and *transient_y_km004_ka002_m0015_p025* show examples of the transient dynamics for the early stages of phenotypic pattern formation. In the videos, the left panels show the spatial patterns for alleles *A* and *B*, respectively, as they are formed through the generations, while the right panels show the values of the frequency of the respective allele (x_k and y_k) for each site, as a function of the sites' index, k (same indexation used before. See Fig. A1(b)), for each generation. The used parameters were $p = 0.25$, $m = 0.015$, $K_M = 0.04$, $K_A = -0.02$ and $Q = 0.02$. From the videos it is clear that even though we simulate for a total time of 40000 generations, the spatial pattern is almost completely formed as early as 3000 generations.

For the pattern of allele *B*, the first 300 generations mark a distinctive separation of the sites into two groups: part of the sites move up faster than the others, which is likely related to the 25% of mutualistic sites, going towards fixation of allele *B*. This clear separation, however, disappears by generation 300 as the neighboring sites start to have an increased effect on them: from this point on it is not possible to distinguish the site's selective regime by looking at the frequency alone.

These results reinforce the argument why the transient dynamics are important: since allele *A* only feels the spatial structure of the mosaic through the interaction with allele *B*, the timescales for the formation of phenotypic patterns for *A* and *B* might be different. The analysis of the dependencies between selection, gene flow and coevolutionary timescales might be an interesting topic for future research.

Literature Cited

- Alonso, D., F. Bartumeus, and J. Catalan. 2002. Mutual interference between predators can give rise to Turing spatial patterns. *Ecology* 83:28–34.
- Anderson, B., and S. D. Johnson. 2008. The geographical mosaic of coevolution in a plant-pollinator mutualism. *Evolution* 62:220–225.
- Benkman, C., and T. Parchman. 2013. When directional selection reduces geographic variation in traits mediating species interactions. *Ecology and evolution* 3:961–970.
- Benkman, C. W., W. C. Holimon, and J. W. Smith. 2001. The influence of a competitor on the geographic mosaic of coevolution between crossbills and lodgepole pine. *Evolution* 55:282–294.
- Benkman, C. W., T. L. Parchman, and E. T. Mezquida. 2010. Patterns of coevolution in the adaptive radiation of crossbills. *Annals of the New York Academy of Sciences* 1206:1–16.
- Brodie, E. D., B. J. Ridenhour, and E. D. Brodie III. 2002. The evolutionary response of predators to dangerous prey: hotspots and coldspots in the geographic mosaic of coevolution between garter snakes and newts. *Evolution* 56:2067–2082.
- Burdon, J. J., and P. H. Thrall. 2014. What have we learned from studies of wild plant-pathogen associations?-the dynamic interplay of time, space and life-history. *European Journal of Plant Pathology* 138:417–429.
- Dybdahl, M. F., and C. M. Lively. 1996. The geography of coevolution: comparative population structures for a snail and its trematode parasite. *Evolution* 50:2264–2275.
- Felsenstein, J. 1976. The theoretical population genetics of variable selection and migration. *Annual review of genetics* 10:253–280.
- Forde, S. E., J. N. Thompson, and B. J. M. Bohannan. 2004. Adaptation varies through space and time in a coevolving host-parasitoid interaction. *Nature* 431:841–844.

- Gandon, S., A. Buckling, E. Decaestecker, and T. Day. 2008. Host-parasite coevolution and patterns of adaptation across time and space. *Journal of evolutionary biology* 21:1861–6.
- Gibert, J. P., M. M. Pires, J. N. Thompson, and P. R. Guimarães. 2013. The spatial structure of antagonistic species affects coevolution in predictable ways. *The American naturalist* 182:578–91.
- Gómez, J. M., F. Perfectti, J. Bosch, and J. P. M. Camacho. 2009. A geographic selection mosaic in a generalized plant-pollinator-herbivore system. *Ecological Monographs* 79:245–263.
- Gómez, P., and A. Buckling. 2011. Bacteria-phage antagonistic coevolution in soil. *Science* 332:106–9.
- Gomulkiewicz, R., J. Thompson, R. Holt, S. Nuismer, and M. Hochberg. 2000. Hot spots, cold spots, and the geographic mosaic theory of coevolution. *American Naturalist* 156:156–174.
- Gotelli, N. J., G. R. Graves, and C. Rahbek. 2010. Macroecological signals of species interactions in the Danish avifauna. *Proceedings of the National Academy of Sciences of the USA* 107:5030–5.
- Guimarães, P. R., M. M. Pires, P. Jordano, J. Bascompte, and J. N. Thompson. 2017. Indirect effects drive coevolution in mutualistic networks. *Nature* 550:511.
- Hanifin, C. T., E. D. Brodie Jr., and E. D. Brodie III. 2008. Phenotypic mismatches reveal escape from arms-race coevolution. *PLoS biology* 6:e60.
- Johnson, S. D. 2010. The pollination niche and its role in the diversification and maintenance of the southern African flora. *Philosophical Transactions of the Royal Society B* 365:499–516.
- King, K. C., L. F. Delph, J. Jokela, and C. M. Lively. 2009. The geographic mosaic of sex and the Red Queen. *Current Biology* 19:1438–41.
- Koskella, B., J. N. Thompson, G. M. Preston, and A. Buckling. 2011. Local biotic environment shapes the spatial scale of bacteriophage adaptation to bacteria. *American Naturalist* 177:440–51.

- Laine, A.-L. 2009. Role of coevolution in generating biological diversity: spatially divergent selection trajectories. *Journal of Experimental Botany* 60:2957–70.
- Lemos-Costa, P., A. B. Martins, J. N. Thompson, and M. A. de Aguiar. 2017. Gene flow and metacommunity arrangement affects coevolutionary dynamics at the mutualism–antagonism interface. *Journal of The Royal Society Interface* 14:20160989.
- Lenormand, T. 2002. Gene flow and the limits to natural selection. *Trends in Ecology & Evolution* 17:183–189.
- Lexer, C., C. Caseys, C. Stritt, and T. G. Whitham. 2013. Integrating the ‘genomic mosaic’ view of species into studies of biotic interactions: A comment on Bernhardsson et al. (2013). *Ecology Letters* 16:1515–e7.
- Lion, S., and S. Gandon. 2015. Evolution of spatially structured host-parasite interactions. *Journal of Evolutionary Biology* 28:10–28.
- Liu, Q.-X., R.-H. Wang, Z. Jin, J. van de Koppel, and D. Alonso. 2010. Spatial self-organization in a multi-strain host–pathogen system. *Journal of Statistical Mechanics: Theory and Experiment* 2010:P05017.
- Murray, J. 2011. *Mathematical Biology II: Spatial Models and Biomedical Applications*. Interdisciplinary Applied Mathematics. Springer New York.
- Nagylaki, T. 1975. Conditions for the existence of clines. *Genetics* 80:595–615.
- Nogueira, A., P. J. Rey, M. Alcántara, Julio, R. M. Feitosa, and L. Lohmann. 2015. Geographic mosaic of plant evolution: Extrafloral nectary variation mediated by ant and herbivore assemblages. *PLoS One* 10.
- Nuismer, S. L., P. Jordano, and J. Bascompte. 2013. Coevolution and the architecture of mutualistic networks. *Evolution* 67:338–354.

- Nuismer, S. L., J. N. Thompson, and R. Gomulkiewicz. 1999. Gene flow and geographically structured coevolution. *Proceedings of the Royal Society B* 266:605–9.
- . 2000. Coevolutionary clines across selection mosaics. *Evolution* 54:1102–1115.
- Parchman, T. L., and C. W. Benkman. 2002. Diversifying coevolution between crossbills and black spruce on Newfoundland. *Evolution* 56:1663–1672.
- Pennings, S. C., C. K. Ho, C. S. Salgado, K. Wieski, N. Davé, A. E. Kunza, and E. L. Wason. 2009. Latitudinal variation in herbivore pressure in Atlantic Coast salt marshes. *Ecology* 90:183–195.
- Raimundo, R. L. G., J. P. Gibert, D. H. Hembry, and P. R. Guimarães. 2014. Conflicting selection in the course of adaptive diversification: the interplay between mutualism and intraspecific competition. *American Naturalist* 183:363–75.
- Rice, S. H. 2004. Evolutionary theory: mathematical and conceptual foundations. Sinauer Associates.
- Ruano, F., S. Devers, O. Sanllorente, C. Errard, A. Tinaut, and A. Lenoir. 2011. A geographical mosaic of coevolution in a slave-making host–parasite system. *Journal of Evolutionary Biology* 24:1071–1079.
- Slatkin, M. 1978. Spatial patterns in the distributions of polygenic characters. *Journal of Theoretical Biology* 70:213–228.
- Thompson, J. 2005. The Geographic Mosaic of Coevolution. Interspecific Interactions. University of Chicago Press, Chicago IL.
- Thompson, J. N. 2013. Relentless evolution. University of Chicago Press, Chicago IL.
- Thompson, J. N., and B. M. Cunningham. 2002. Geographic structure and dynamics of coevolutionary selection. *Nature* 417:735–8.

- Thompson, J. N., and K. F. Merg. 2008. Evolution of polyploidy and the diversification of plant-pollinator interactions. *Ecology* 89:2197–2206.
- Toju, H., H. Abe, S. Ueno, Y. Miyazawa, F. Taniguchi, T. Sota, and T. Yahara. 2011. Climatic gradients of arms race coevolution. *American Naturalist* 177:562–73.
- van Valen, L. 1973. A new evolutionary law. *Evolutionary Theory* 1:1–30.
- Vogwill, T., A. Fenton, A. Buckling, M. E. Hochberg, and M. a. Brockhurst. 2009. Source populations act as coevolutionary pacemakers in experimental selection mosaics containing hotspots and coldspots. *American Naturalist* 173:E171–6.
- Wade, M. J. 2007. The co-evolutionary genetics of ecological communities. *Nature Reviews Genetics* 8:185–95.
- Whitham, T. G., J. K. Bailey, J. A. Schweitzer, S. M. Shuster, R. K. Bangert, C. J. LeRoy, E. V. Lonsdorf, G. J. Allan, S. P. DiFazio, B. M. Potts, D. G. Fischer, C. a. Gehring, R. L. Lindroth, J. C. Marks, S. C. Hart, G. M. Wimp, and S. C. Wooley. 2006. A framework for community and ecosystem genetics: from genes to ecosystems. *Nature Reviews Genetics* 7:510–23.

Figure legends

Figure 1: Final stationary patterns of x (frequency of allele A), for three values of the gene flow rate, m , and different selection mosaics (each mosaic defined by the probability of a site to be mutualistic, p). The three final patterns in each row correspond to the same selection mosaic in the left. The other parameters are $K_M = 0.04$, $K_A = -0.02$ and $Q = 0.02$ and each pattern is iterated over 40000 generations.

Figure 2: Final stationary patterns of y (frequency of allele B), for three rates of gene flow, m , and different selection mosaics (each mosaic defined by the probability of a site to be mutualistic, p). Patterns correspond to the coevolutionary model (both x and y vary in time). Selection mosaics and parameters are the same as in Fig. 1. Each simulation ran for 40000 generations.

Figure 3: Final stationary patterns of y (frequency of allele B), corresponding to the single-species model (frequency of allele A is fixed as $x = 1$ at all sites), for three rates of gene flow, m , and different selection mosaics, with probability p for sites where selection is beneficial. Sites where selection is detrimental (det; fitness of allele B equals $1 - |K_A|$) or beneficial (ben; fitness of allele B equals $1 + |K_M|$), correspond to the position of antagonistic or mutualistic sites, respectively, on the mosaics of Figs. 1 and 2. Parameters are the same used in the previous figures. Each simulation ran for 40000 generations.

Figure 4: In (a), average fraction of sites on the lattice for which $x > 0.7$ as a function of the gene flow m , for different values of the proportion of mutualistic sites, p . For each value of m , 50 samples were considered and error bars correspond to one standard deviation. In (b), results for the mean-field approach, with values of C_{AV} as a function of the gene flow m , for different size ratios of mutualistic to antagonistic communities, $R = N_1/N_2$.

Figure 5: Cluster size frequencies for alleles A (a) and B (b), for four different values of gene flow, m , for cluster of sites in which the allele frequency is greater than 0.7 (see description in Methods). Each point represents the number of clusters with that size normalized by the total clusters count. For each rate of gene flow, 1000 different selection mosaics (error bars equal to the standard error of the mean) with $p = 0.25$ were considered. Empty diamonds show the same cluster analysis considering the mutualistic clusters on the selection mosaic. Arrows represent the mean cluster size for each value of m (using the same color legends). As before, $K_M = 0.04$, $K_A = -0.02$ and $Q = 0.02$.

Figure 6: Average fraction of sites on the lattice that present final values $x_{ij} > 0.7$ for different values of gene flow, m , and the fraction of coldspots, f , on the lattice. The average fitness sensitivity for the host, $\overline{s_{YC}}$, is fixed in each case, with values -0.005 (a), 0.0 (b), and 0.005 (c). The original lattices are constructed with p for the initial selection mosaic varying with f according to Eq. 9. Ten simulations for each pair (m, f) were performed. For all cases, $K_M = 0.04$, $K_A = -0.02$ and $Q = 0.02$.

Online figure legends

Figure A1: In (a), selection block mosaic, where the lower half of the lattice is composed only by antagonistic sites, while the upper half is composed by mutualistic sites. In (b), average value of the frequency of allele A (x_k) for the 20% last iteration steps (total iteration time equal 40000), as a function of the node indexes, k , for different values of the gene flow rate, m . Here we use $K_M = 0.04$, $K_A = -0.02$ and $Q = 0.02$.

Figure A2: Final outcomes for the spatial distribution of allele A on the block mosaic, for different gene flow rates, corresponding to the curves in Fig. A1(b). For these patterns, $m = 0.060$ (a), $m = 0.100$ (b), $m = 0.250$ (c) and $m = 0.500$ (d).

Figure A3: Visualization of the gradient selection mosaic. For each row i , indexing from the bottom to the top, the sites in this row are assigned mutualistic with a probability $p = i/L$, where $L = 100$ is the size of the lattice. A selection gradient is thus created so that, in each row, the probability for the sites to be mutualistic goes from 0.01 (bottom of the lattice) to 1 (top of the lattice).

Figure A4: Stationary outcomes for the spatial distribution of allele A , for different gene flow rates. For these patterns, $m = 0.015$ (a), $m = 0.050$ (b), $m = 0.100$ (c) and $m = 0.250$ (d). All the cases have the same selection mosaic (Fig. A3). Parameters are the same as before.

Figure A5: Cluster size frequencies for allele B for the coevolutionary (a) and single-species (b) models, for four different values of gene flow, m , for cluster of sites in which the allele frequency is $y > 0.7$. Each point represents the number of clusters with that size normalized by the total clusters count. For each rate of gene flow, 1000 different selection mosaics (error bars equal to the standard error of the mean) with $p = 0.25$ were considered. Empty diamonds show the same cluster analysis considering the mutualistic clusters on the selection mosaic. As before, $K_M = 0.04$, $K_A = -0.02$ and $Q = 0.02$.

Figure A6: Cluster size frequencies for allele B for the coevolutionary (a) and single-species (b) models, for four different values of gene flow, m , for cluster of sites in which the allele frequency is $0.3 < y < 0.7$. Inset in (a) shows a zoom of the final interval in that plot. Again, each point is the number of clusters normalized by the total clusters count. For each rate of gene flow, 1000 different selection mosaics (error bars equal to the standard error of the mean) with $p = 0.25$ were considered. Parameters are the same used in Fig. A5.

Video A1: Gene flow effect. See description in Supplementary Material.

Video A2: Transient dynamics, Allele A. See description in Supplementary Material.

Video A3: Transient dynamics, Allele B. See description in Supplementary Material.

Figure 1

Copyright The University of Chicago 2019. Preprint (not copyedited or formatted).
Please use DOI when citing or quoting. DOI: 10.1086/704157

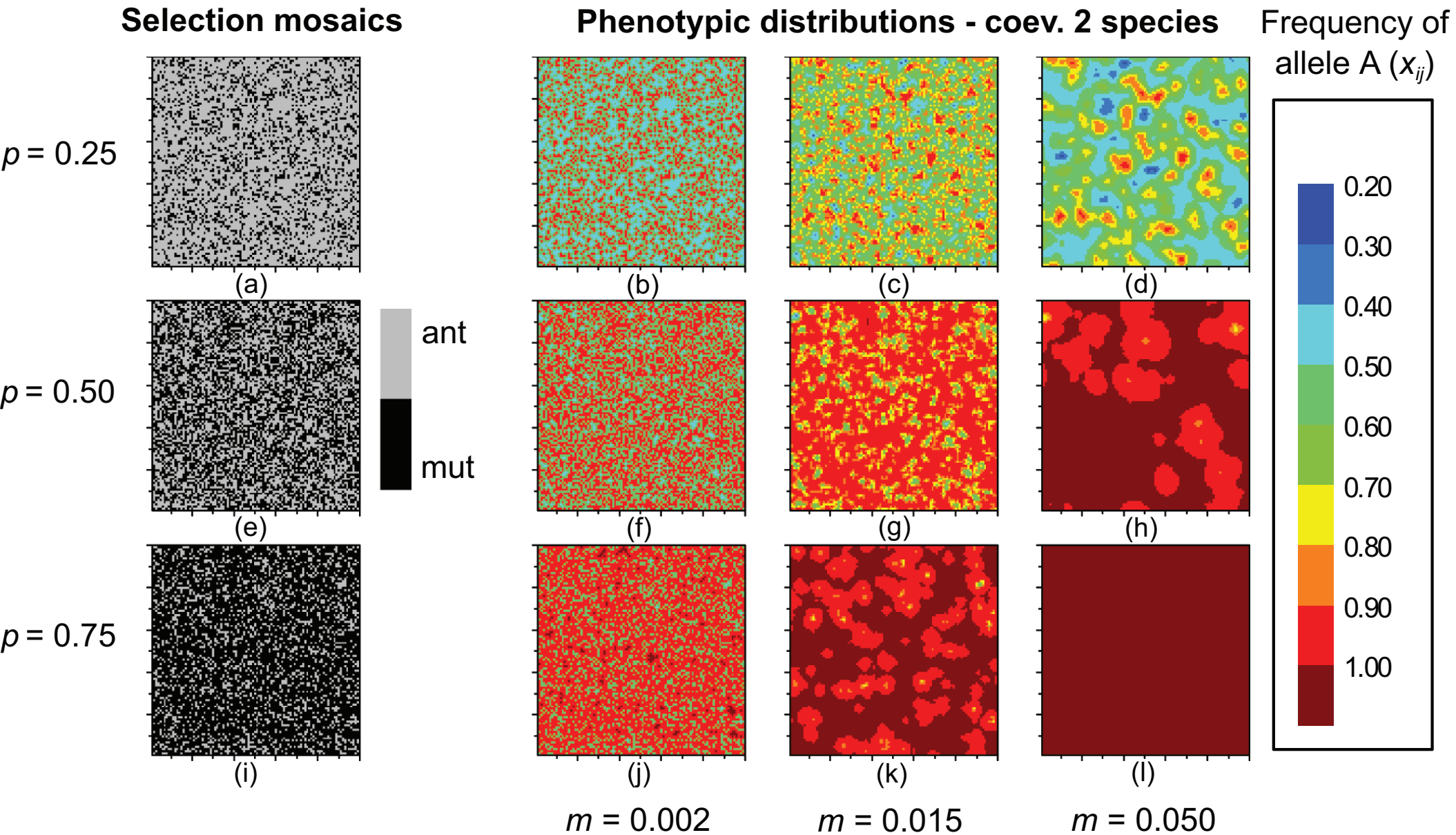


Figure 2

Copyright The University of Chicago 2019. Preprint (not copyedited or formatted).
Please use DOI when citing or quoting. DOI: 10.1086/704157

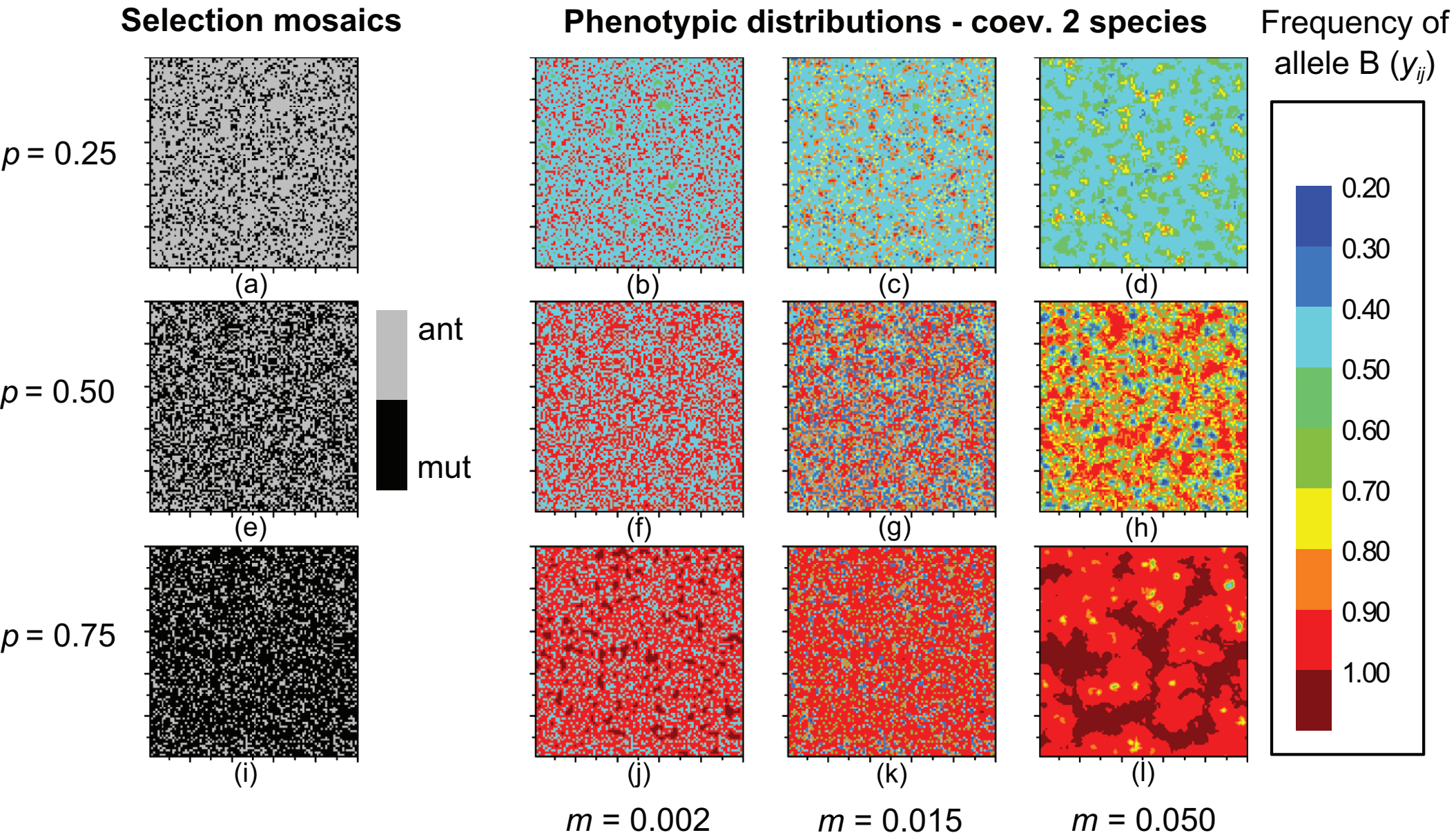


Figure 3

Copyright The University of Chicago 2019. Preprint (not copyedited or formatted).
Please use DOI when citing or quoting. DOI: 10.1086/704157

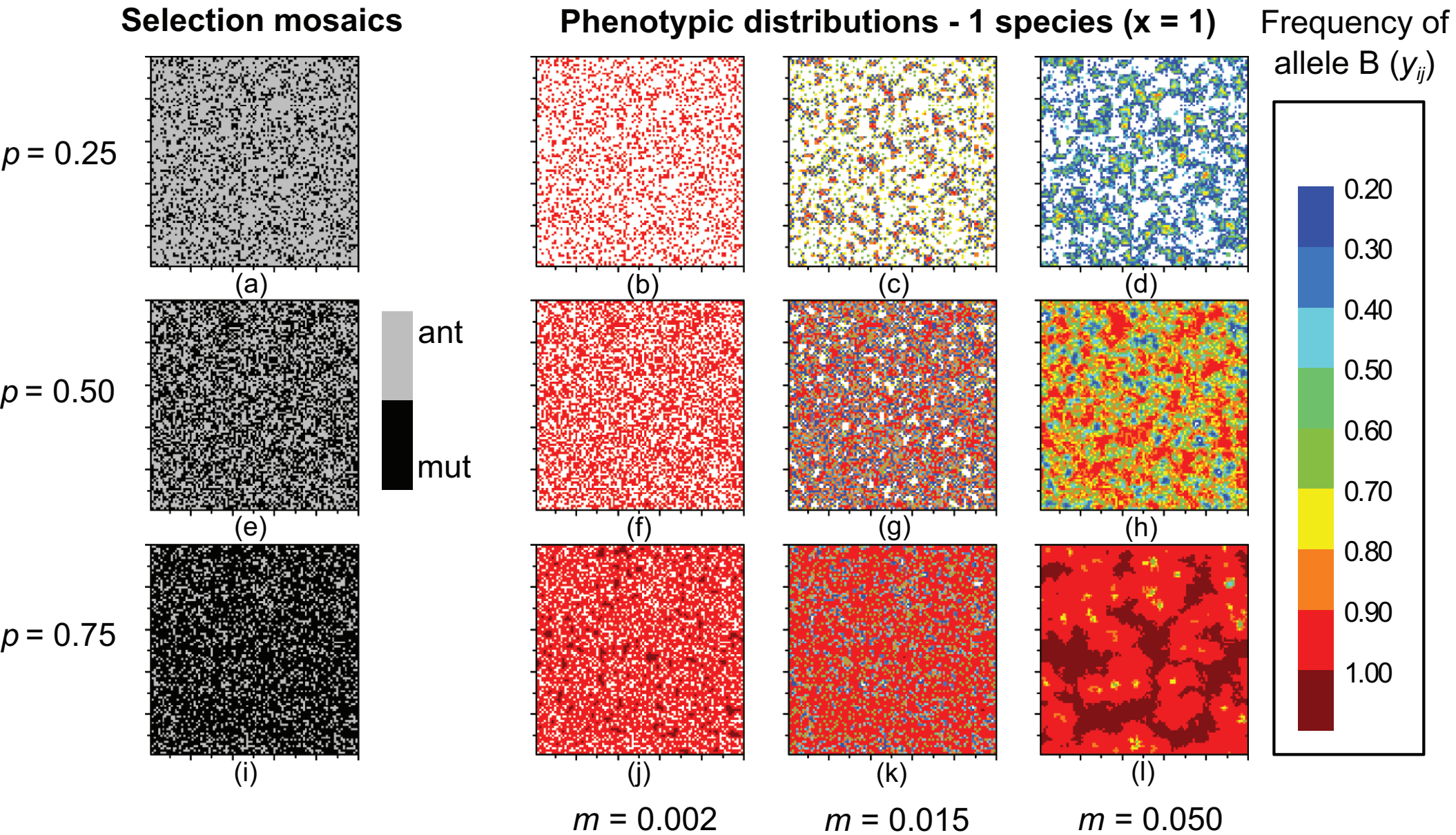


Figure 4

Copyright The University of Chicago 2019. Preprint (not copyedited or formatted).
 Please use DOI when citing or quoting. DOI: 10.1086/704157

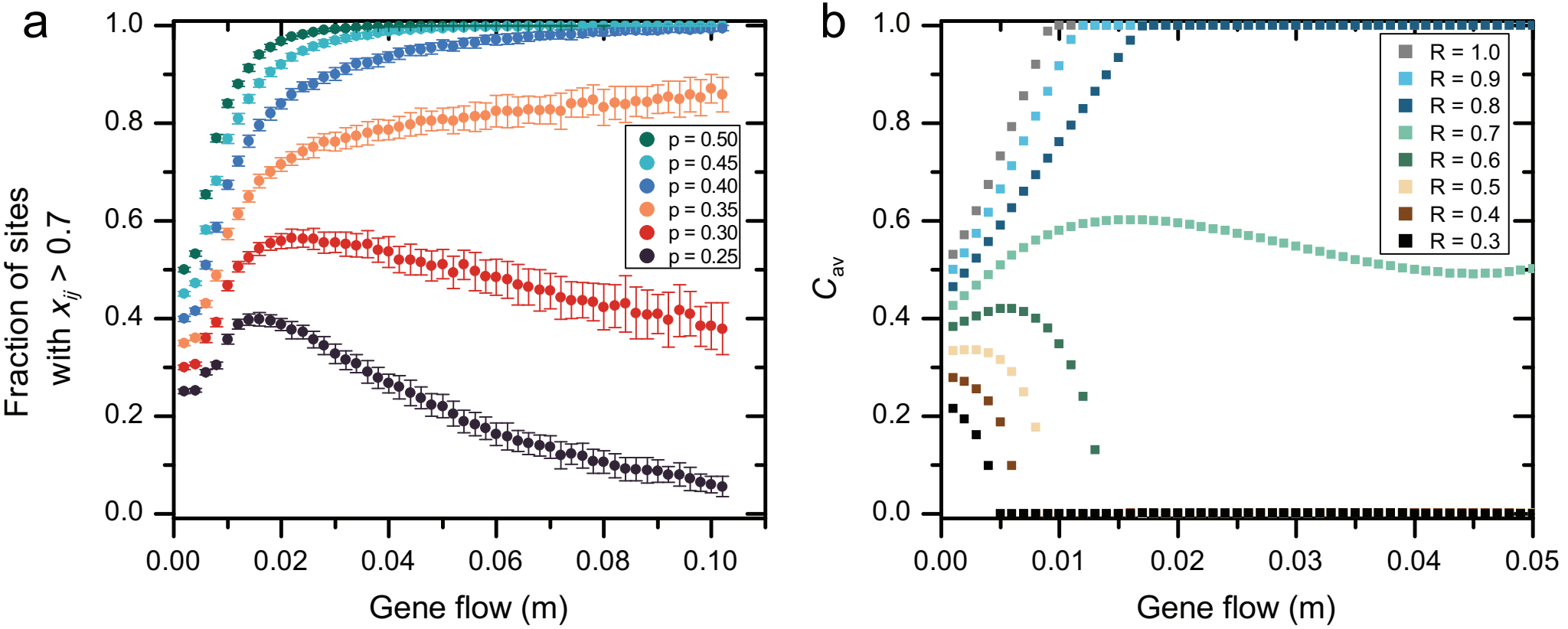


Figure 5

Copyright The University of Chicago 2019. Preprint (not copyedited or formatted).
Please use DOI when citing or quoting. DOI: 10.1086/704157

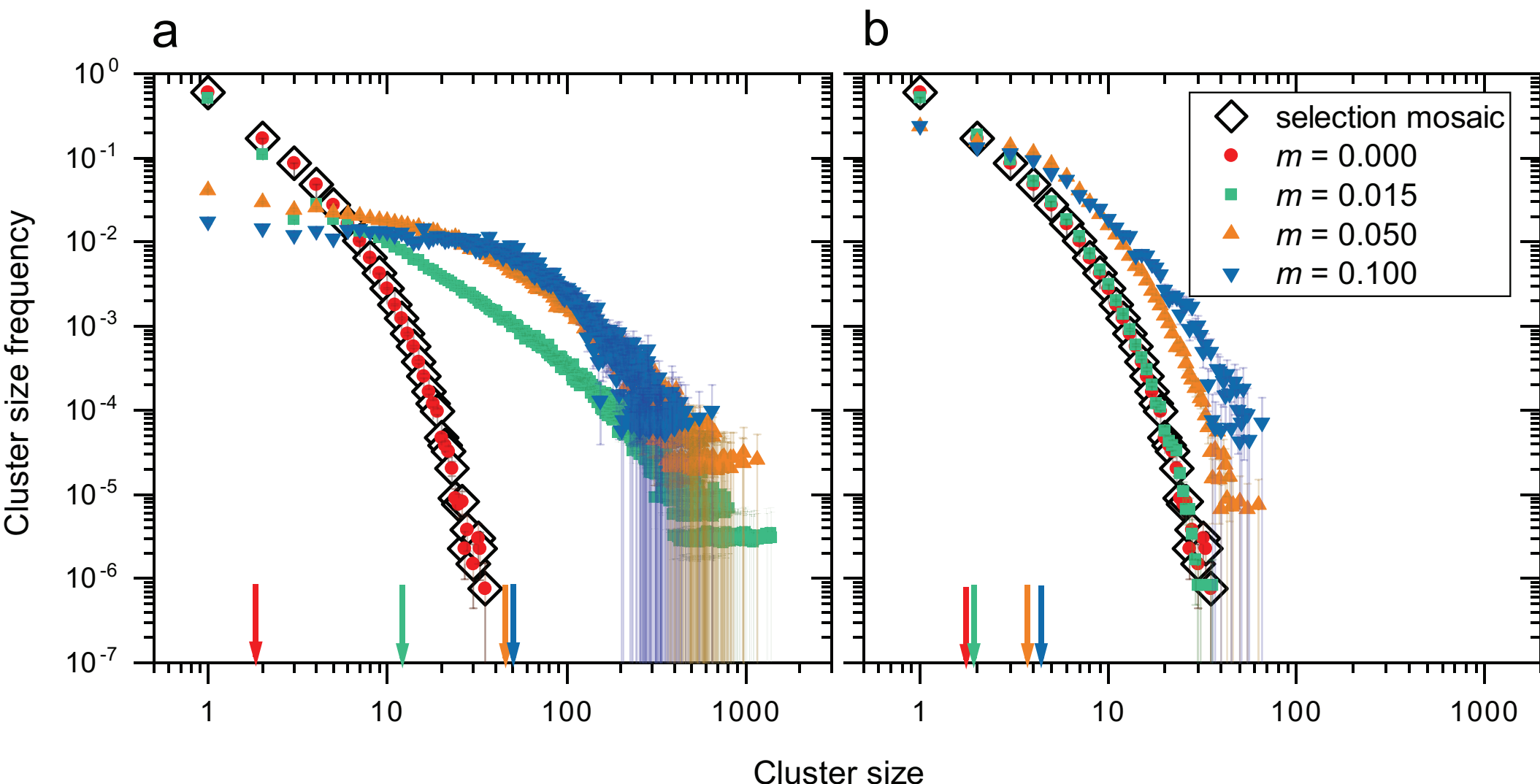


Figure 6

Copyright The University of Chicago 2019. Preprint (not copyedited or formatted).
Please use DOI when citing or quoting. DOI: 10.1086/704157

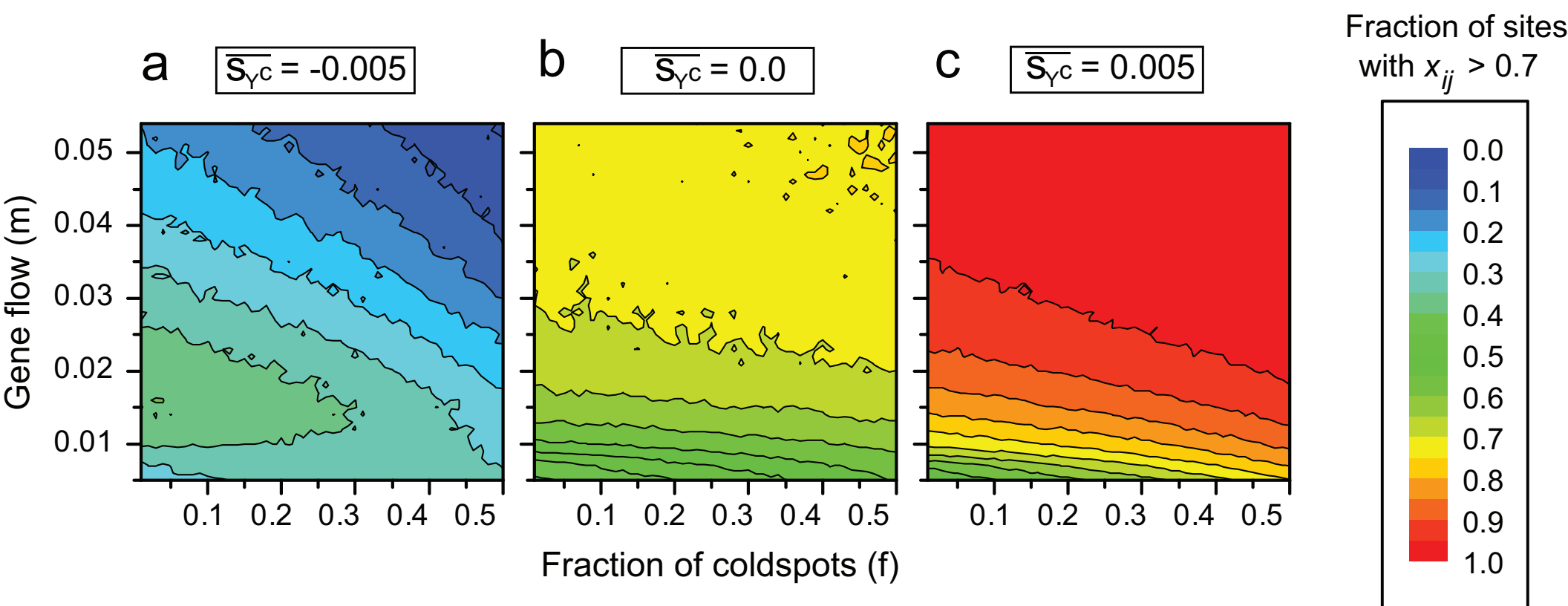
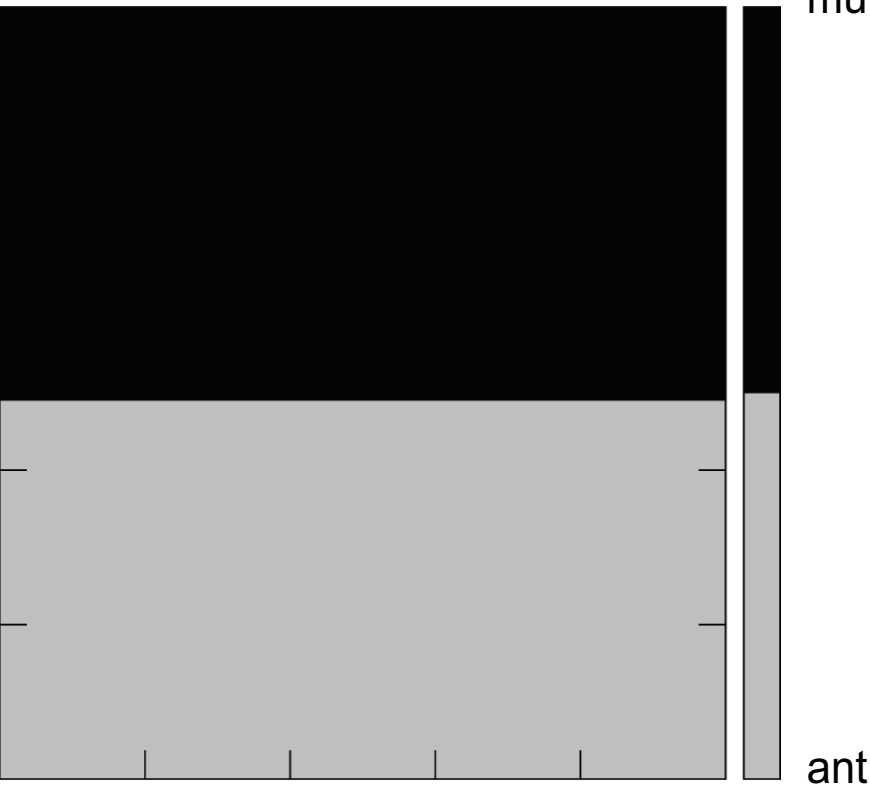


Figure A1

Copyright The University of Chicago 2019. Preprint (not copyedited or formatted).
Please use DOI when citing or quoting. DOI: 10.1086/704157

a



b

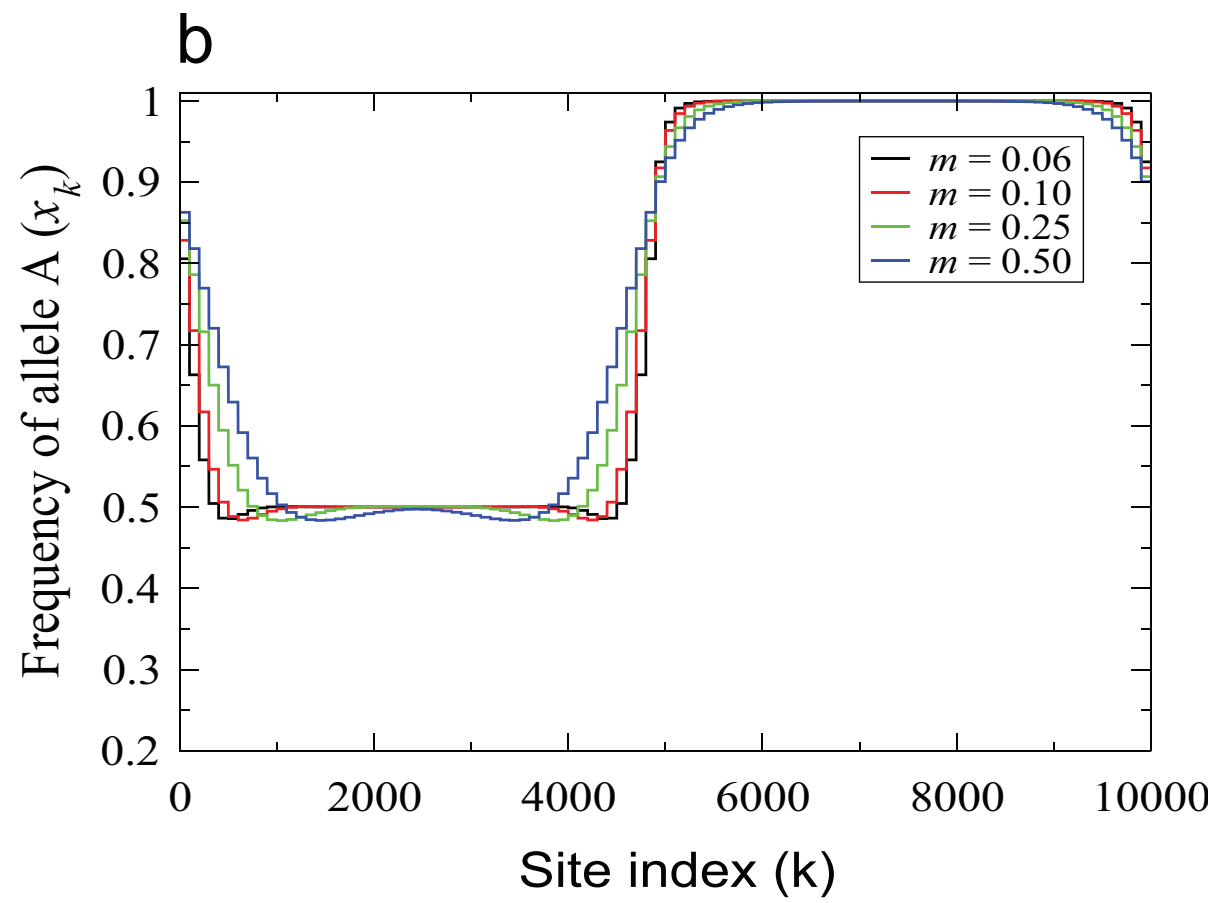
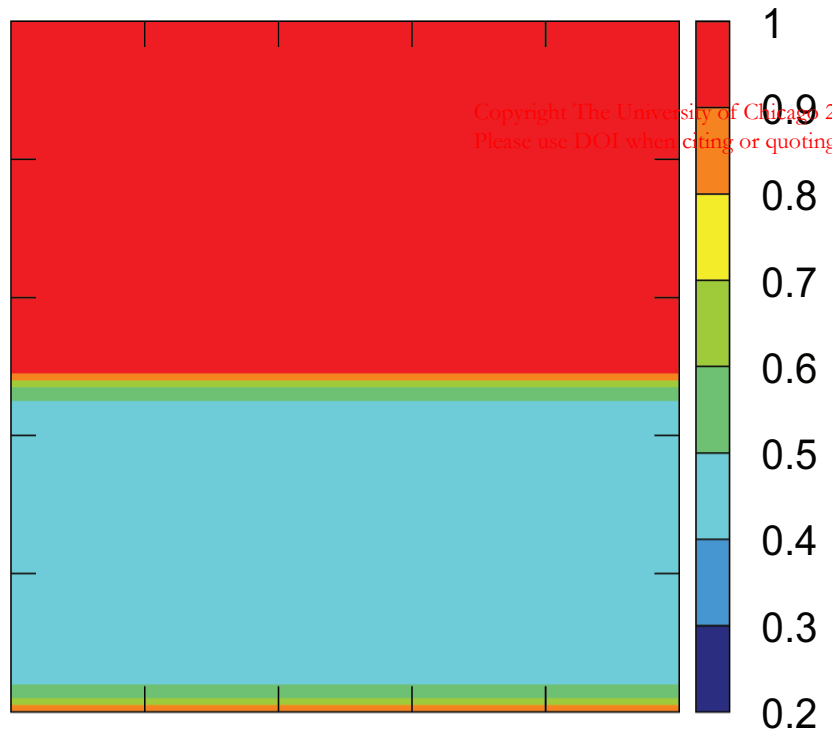
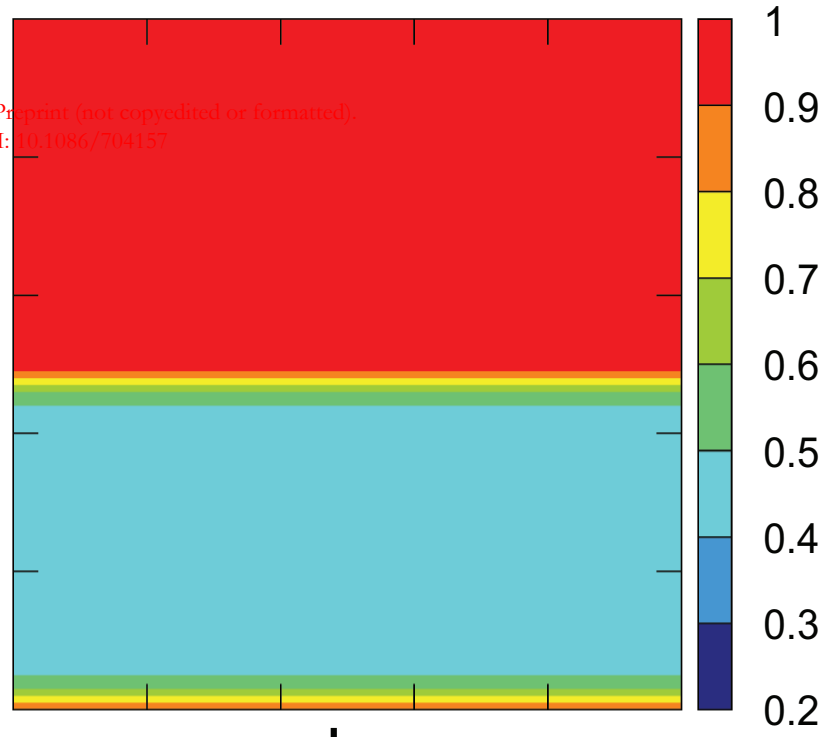


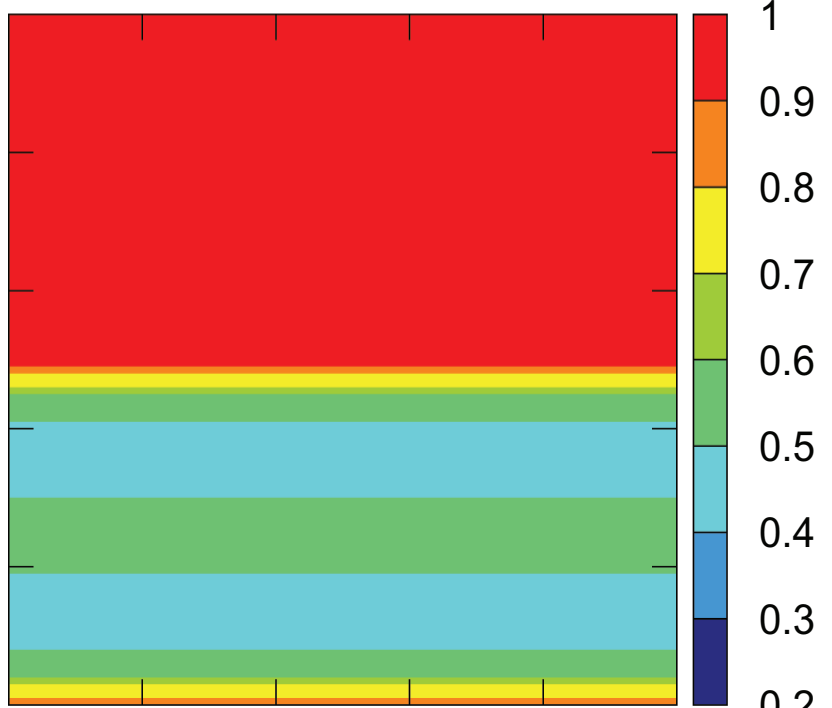
Figure A2



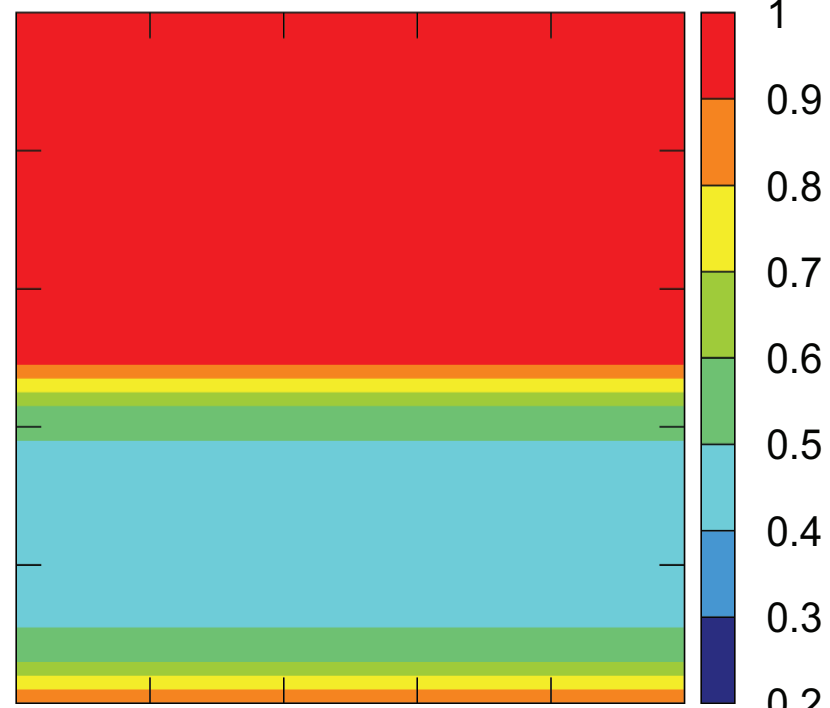
a



b



c



d

Figure A3

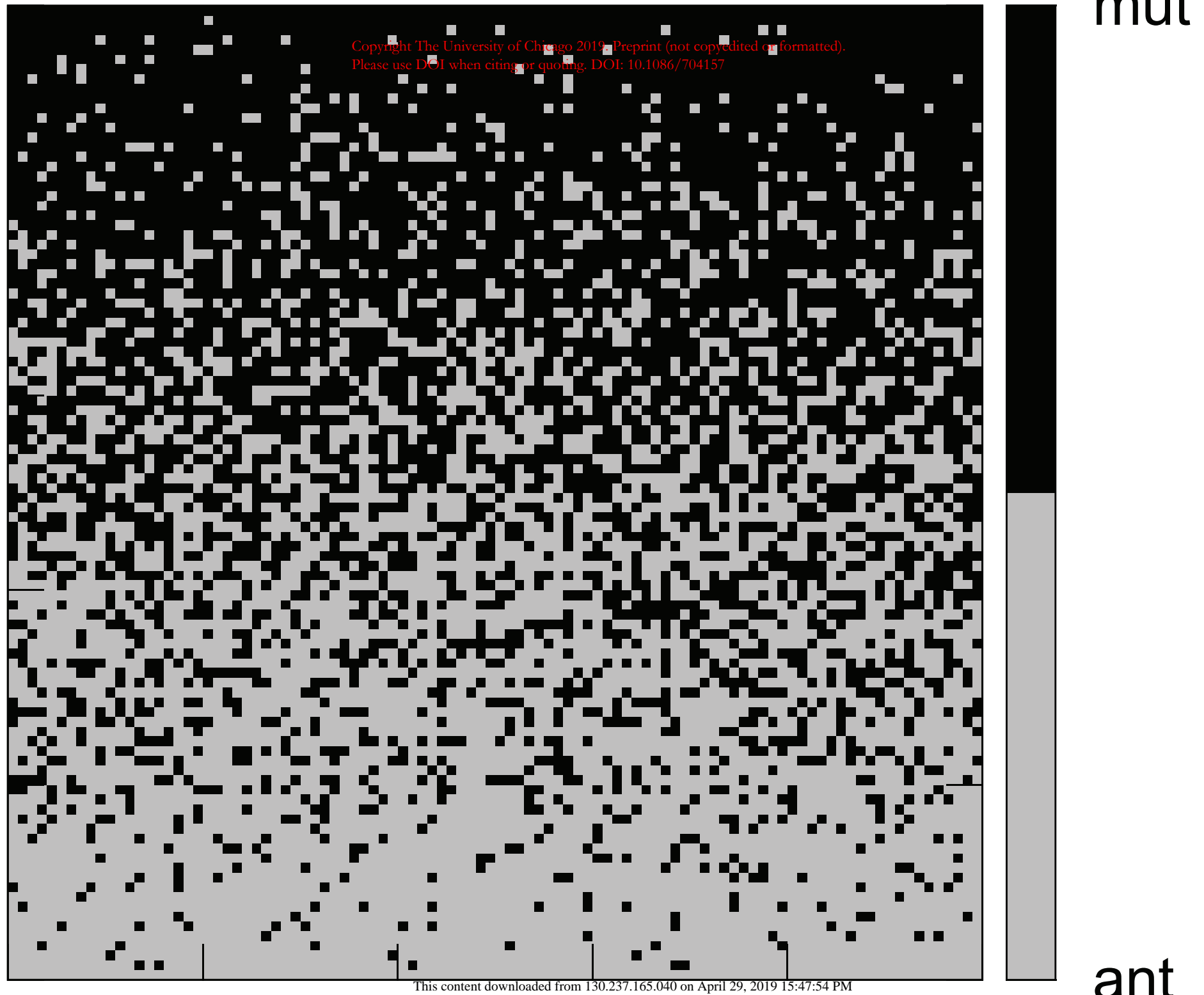


Figure A4

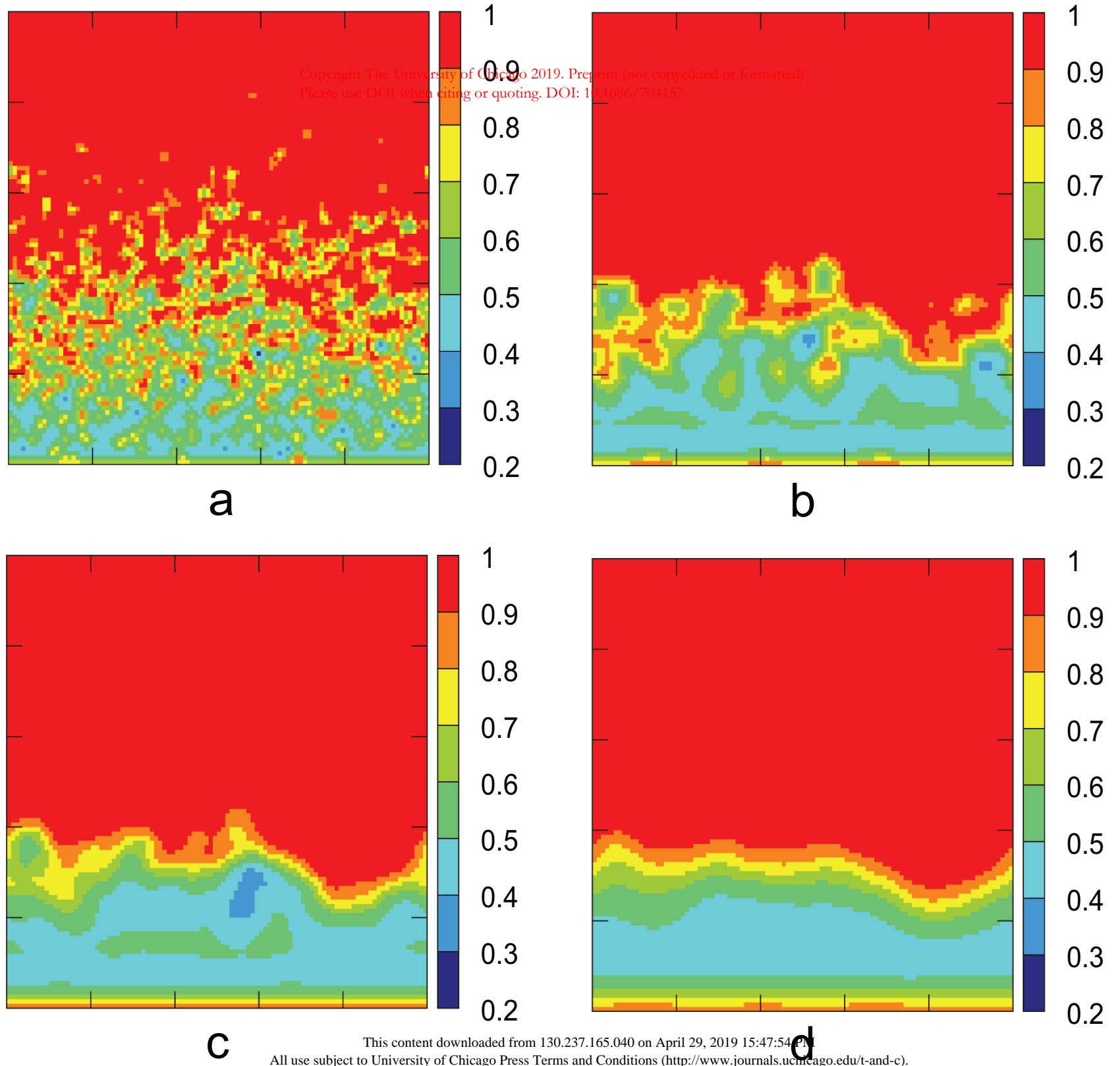


Figure A5

Copyright The University of Chicago 2019. Preprint (not copyedited or formatted).
Please use DOI when citing or quoting. DOI: 10.1086/704157

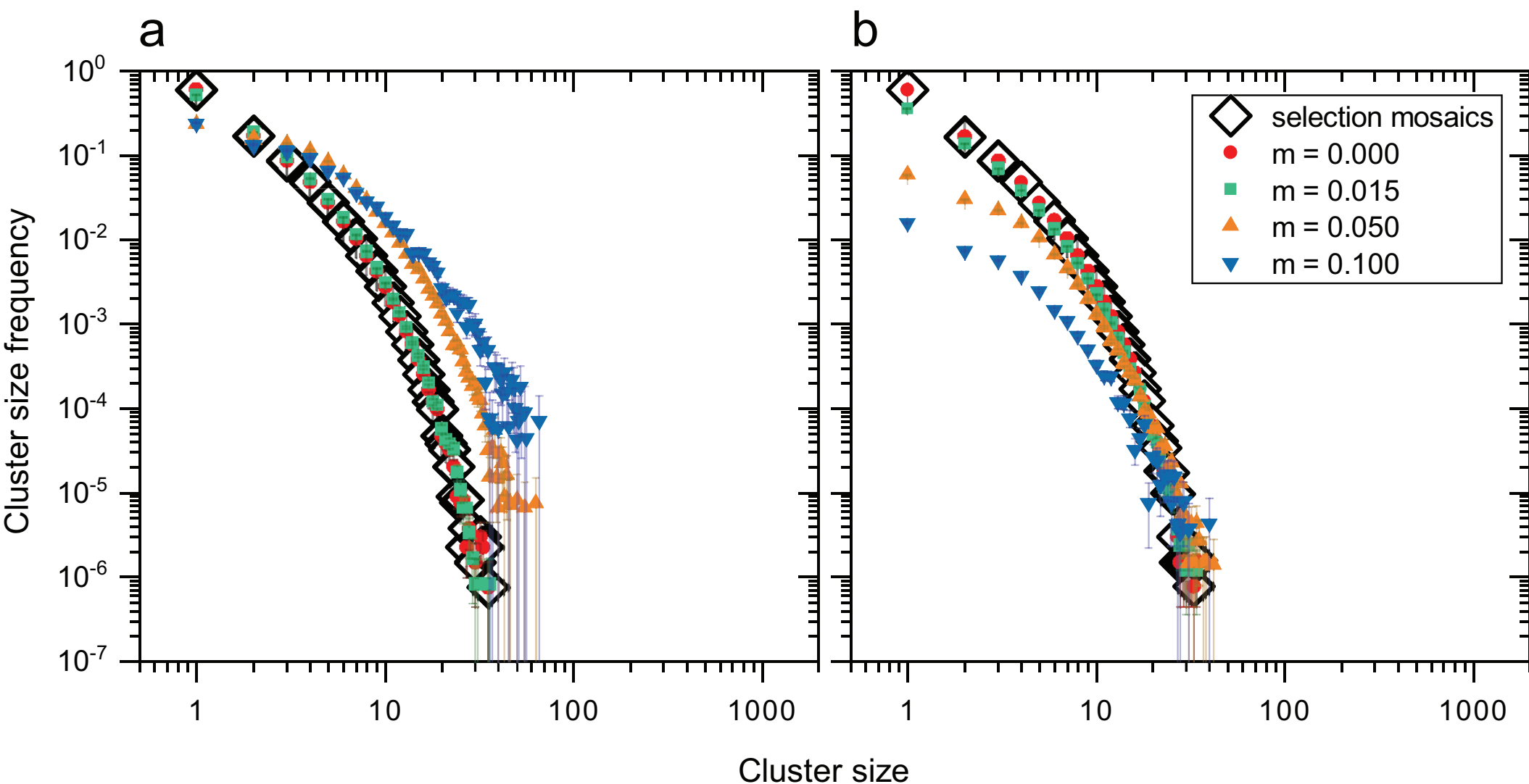
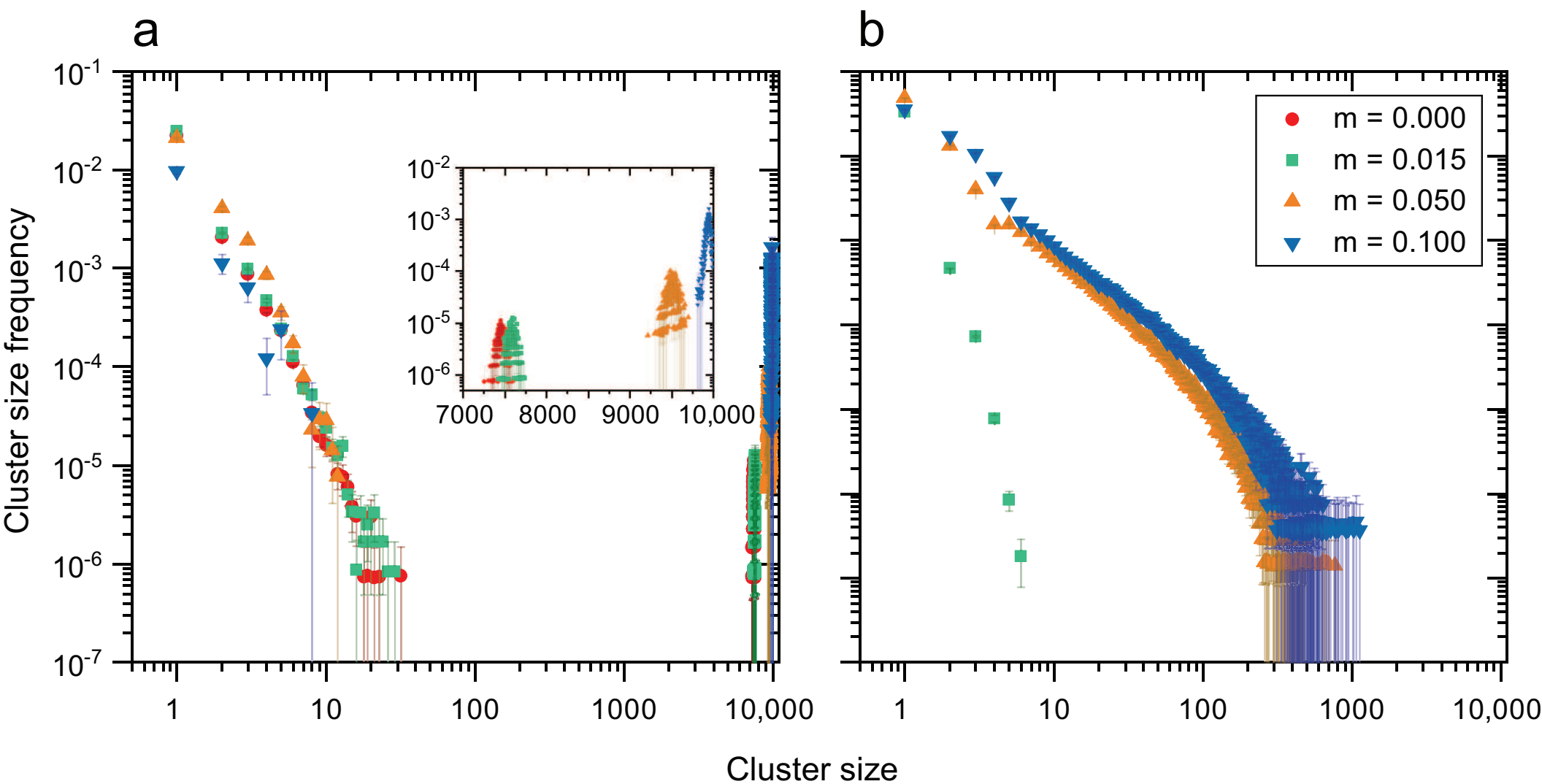


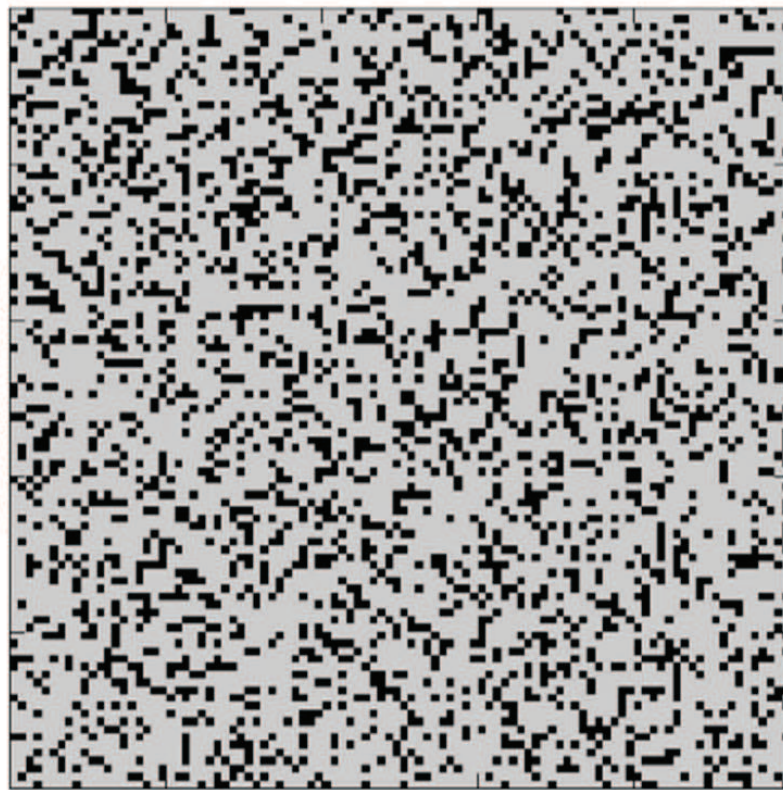
Figure A6

Copyright The University of Chicago 2019. Preprint (not copyedited or formatted).
 Please use DOI when citing or quoting. DOI: 10.1086/704157



$K_W = 0.04; K_A = 0.02; C = 0.02; p = 0.25$

Selection mosaic

gene flow: $m = 0.015$

Final phenotypic distribution

